THE EFFECTS OF CALCIUM ON NF-κB PATHWAY IN HACAT CELLS CONTAINING CONNEXIN26 KID SYNDROME MUTATIONS

A Thesis Submitted to
the Graduate School of
İzmir Institute of Technology
in Partial Fulfillment of the Requirement for the Degree of

MASTER OF SCIENCE

in Molecular Biology and Genetics

by
Sümeyye Şüheda Yaşarbaş

October 2023
İZMİR

We approve the thesis of **Sümeyye Şüheda YAŞARBAŞ**

Examining Committee Members

_____
Assoc. Prof. Dr. Gülistan MEŞE ÖZÇİVİCİ
Department of Molecular Biology and Genetics,
İzmir Institute of Technology

_____
Prof. Dr. Özden YALÇIN ÖZUYSAL
Department of Molecular Biology and Genetics,
Izmir Institute of Technology

_____
Dr. Yavuz OKTAY
Izmir Biomedicine and Genome Center,
Dokuz Eylül University

27 October 2023

_____
Assoc. Prof. Dr. Gülistan MEŞE ÖZÇİVİCİ
Supervisor, Molecular Biology and Genetics,
İzmir Institute of Technology

_____
Prof. Dr. Özden YALÇIN ÖZUYSAL
Head of the Molecular Biology and
Genetics Program

_____
Prof. Dr. Mehtap EANES
Dean of the Graduate School of
Engineering and Sciences

ACKNOWLEDGEMENT

I would like to express my deepest and most sincere gratitude to my supervisor, Assoc. Prof. Dr. Gülistan MEŞE ÖZÇİVİCİ, for her unwavering trust, understanding, and guidance. Her principled stance as a remarkable woman has always been a source of inspiration. I extend my heartfelt thanks for her invaluable contributions to this study, including her critical discussions and invaluable advice.

I am grateful to Prof. Dr. Engin ÖZÇİVİCİ and Prof. Dr. Özden YALÇIN ÖZUYSAL for their critical comments, which significantly enriched this study.

I owe a debt of gratitude to Yağmur Ceren Ünal, whose mentorship has been instrumental in shaping my knowledge and skills. Her enduring patience and guidance have been invaluable to my academic growth.

My gratitude extends to the members of my laboratory who have supported me throughout this journey. Special thanks to Ece İnal, Meryem Azra Yıldırım, Öykü Sarıgil, Yaren Sert and Şüheda Özek for their support and valuable contributions.

I am grateful to Eyüp Yöndem and Arwa Burgeia for their steadfast guidance and support, which have been instrumental in my research endeavours. I would like to thank Doğaç İpekgil and Arda Ceylan for their unwavering support and guidance, which have played a pivotal role in my academic pursuits.

I extend my gratitude to Dane Rusçuklu from IZTECH TAM CFB for her assistance with data measurements.

I have a special place in my heart for my family, as their continued support has been instrumental in all areas of my life. I owe an immeasurable debt of gratitude to my mother, Elif Özer, my father, Ümit Yaşarbaş, and my brother, M. Sungur Yaşarbaş, for being with me every step of the way. I also extend my heartfelt thanks to Baybora Topaloğlu and Azem Berivan Adıbelli for their unwavering support, their belief in my decisions, and their boundless love.

I would like to thank TÜBİTAK for the BIDEB 2210-A scholarship that supported my academic journey. This thesis is funded by TÜBİTAK under grant no. 119Z284.

ABSTRACT

THE EFFECTS OF CALCIUM ON NF-κB PATHWAY IN HACAT CELLS CONTAINING CONNEXIN26 KID SYNDROME MUTATIONS

Keratitis-ichthyosis-deafness (KID) syndrome is a rare genetic disorder characterized by deafness, corneal defects, and thickened, scaly skin and associated with mutations in Connexin26 (Cx26), resulting in the formation of hyperactive hemichannels that disrupt calcium (Ca^{2+}) transfer. Ca^{2+} is crucial for normal epidermal cell function and may contribute to characteristics of KID syndrome. While unregulated Ca^{2+}transfer through aberrant Cx26 hemichannels is known to impact keratinocyte proliferation and differentiation, the specific mechanisms remained unclear. An increase in the molecules associated with the nuclear factor-κB (NF-κB) signaling pathway was observed in the D50Y mutation of KID syndrome. This suggests that Cx26 mutant channels may disrupt keratinocyte physiology through NF-κB signaling. Our study hypothesizes that Ca^{2+} signals altered due to Cx26 mutations affect the NF-κB pathway, potentially contributing to KID syndrome by modifying keratinocyte cell physiology.

Our study showed that NF-κB activation significantly increased in D50Y cells, linked to hyperproliferation and activation was dependent on intracellular Ca^{2+}. This was associated with increased p65 activation and nuclear localization due to hyperactive Cx26 channels in D50Y cells. These findings reveal a direct link between aberrant Ca^{2+}transport through Cx26 channels due to the D50Y mutation and NF-κB activation, shedding light on the hyperproliferative characteristics of Cx26 D50Y KID syndrome.

Our goal was to understand how Ca^{2+} mechanisms impact the NF-κB pathway, potentially altering the physiology of keratinocytes expressing D50Y and G45E mutations. This research offers insights into the potential targeting of the NF-κB pathway for treating KID syndrome caused by Cx26 mutations.

ÖZET

CONNEXIN 26 KID SENDROMU MUTASYONLARINI İÇEREN HACAT HÜCRELERİNDE KALSİYUMUN NF-κB YOLAĞI ÜZERİNEKİ ETKİLERİ

Keratitis-ichthyosis-deafness (KID) sendromu, sağırlık, kornea defektleri ve kalınlaşmış ve pullu cilt ile karakterize edilen, Connexin26 (Cx26) mutasyonlarıyla ilişkili, kalsiyum (Ca^{2+}) transferini bozan hiperaktif hemikanalların oluşumuyla sonuçlanan ve nadir görülen bir genetik hastalıktır. Normal epidermal hücre fonksiyonu için kritik öneme sahip olan Ca^{2+}, KID sendromunun karakteristiklerine katkıda bulunabilir. Anormal Cx26 kanalları yoluyla düzensiz Ca^{2+} aktarımının keratinosit proliferasyonunu ve farklılaşmasını etkilediği bilinmesine rağmen bunu gerçekleştiren mekanizmalar belirsizliğini korumuştur. KID sendromunun D50Y mutasyonunda, nükleer faktör-κB (NF-κB) sinyal yolağı ile ilişkili moleküllerde artış gözlenmiştir. Bu, Cx26 mutant kanallarının NF-κB sinyallemesi yoluyla keratinosit fizyolojisini bozabileceğini göstermektedir. Araştırmamız, Cx26 mutasyonları nedeniyle değişen Ca^{2+} sinyallerinin NF-κB yolağını etkilediğini ve keratinosit hücre fizyolojisini değiştirerek KID sendromuna katkıda bulunabileceği hipotezini öne sürmektedir.

Araştırmamız, hiperproliferasyonla bağlantılı olarak D50Y hücrelerinde NF-κB aktivasyonunun önemli ölçüde arttığını ve aktivasyonun hücre içi Ca^{2+}'ya bağlı olduğunu göstermiştir. Bu durum, D50Y hücrelerindeki hiperaktif Cx26 kanallarına bağlı olarak artan p65 aktivasyonu ve nükleer lokalizasyonu ile ilişkilendirilmiştir. Bu bulgular, D50Y mutasyonu kaynaklı olarak Cx26 kanalları boyunca anormal Ca^{2+} taşınması ile NF-κB aktivasyonu arasında doğrudan bağlantı olduğunu göstermekte ve Cx26 D50Y KID sendromunun hiperproliferatif özelliklerine ışık tutmaktadır.

Buradaki amacımız, Ca^{2+} mekanizmalarının NF-κB yolağını nasıl etkilediğini ve D50Y ile G45E mutasyonlarını eksprese eden keratinositlerin fizyolojisini nasıl değiştirebileceğini anlamaktı. Bu araştırma, Cx26 mutasyonlarının neden olduğu KID sendromunun tedavisi için NF-κB yolağına yönelmenin mümkün olabileceğine dair bilgiler sunmaktadır.

To all women,

To all people deprived of their fundamental rights

TABLE OF CONTENTS

LIST OF FIGURES

Figure **Page**

Figure **Page**

Figure **Page**

LIST OF TABLES

Table **Page**

CHAPTER 1

INTRODUCTION

1.1 The Skin

The skin is a barrier against physical, chemical, and mechanical traumas and pathogens. The two layers of the skin, the dermis and the epidermis are separated by the basement membrane. The dermis and hypodermis are connective tissues while the epidermis is composed of epithelial keratinocytes. The epidermis is responsible for forming a barrier to regulate molecular exchange and to protect against environmental threats. The epidermis has 4 layers; stratum basale (inner surface), stratum spinosum, stratum granulosum, and stratum corneum (outer surface). Stratum corneum is the outermost layer composed of flattened dead keratinocytes providing a barrier against environmental factors. Stratum granolusum provides lipid production for preventing water loss. Stratum spinosum is composed of keratinocytes and provides flexibility to skin and has roles in immune response. The basal layer consists of new keratinocytes formed through cell proliferation (Blanpain & Fuchs, 2006; Mese et al., 2011; Abdo et al., 2020). The stratum corneum provides physical, biochemical, and adaptive immune barriers. The physical barrier is mainly composed of adherens and tight junctions for reconstruction of the integrated barrier. The chemical barrier is provided by low pH levels of the corneum with the accumulation of free fatty acids. The antimicrobial barrier protects from external aggressions by interaction with immune cells (Garcia-Vega et al., 2021; H. J. Lee & Kim, 2022). The basal layer includes stem cells, and these stem cells divide and differentiate into keratinocytes of the outer layer. During the differentiation of these cells, many changes are observed at both protein and structural levels. Many protein pathways, basement membrane components, Ca^{2+} balance and adhesion molecules have been revealed to play roles in these cellular events (Fuchs, 2008).

1.2 Gap Junctions in the skin

Gap junctions are specialized connections that facilitate direct intercellular communication by transporting ions, amino acids, secondary messengers, and short interfering RNAs between adjacent cells (Goodenough & Paul, 2009; Aypek et al., 2016) (Figure 1.1). Intercellular communication plays roles in many physiological events including proliferation, differentiation, and cellular homeostasis. Gap junctions are composed of connexin (Cx) gene family in chordates and have a rapid turnover to respond to the changes in the extracellular environment. In humans, 21 different Cx isoforms are found and classified by their molecular weight ranging between 23 and 62 kDa (Refs). Cxs is found in every tissue of the human body and more than one subtype of Cxs is also seen in most of the cell types. For instance, Cx26 is expressed in the epidermis, appendages, visual cortical neurons, cochlea etc. Also, more than one Cx type can be expressed in a single type of cell, such as Cx26 and Cx32 in liver cells (Garcia, 2021). Cxs have four alpha helical transmembrane domains, two extracellular loops, one cytoplasmic loop where variations mostly occur (Figure 1.1.b) (Faniku et al., 2015; Garcia-Vega et al., 2021).

Gap junctions' biosynthesis occurs by the oligomerization of six Cx subunits into hemichannels or connexons in ER-Golgi network (Aasen et al., 2018) (Figure 1.1.a). Hemichannels can be formed either homomeric by the oligomerization of the same type of Cx subunits or heteromeric as a result of the oligomerization of the different types of Cx subunits. Then, they are transported to the plasma membrane to align with other connexons from adjacent cells or individually function as hemichannels (Figure 1.1.c, d, e). In addition to hemichannels, gap junction channels can be homotypic or heterotypic based on their connexon composition (Figure 1.1.d) (Donahue et al., 2018). These hemichannels release different compounds smaller than 1.4 kDa including Ca^{2+}, cAMP, ATP, and microRNAs by opening under both normal and abnormal physiological conditions (Evans et al., 2006; Goodenough & Paul, 2009). In addition to these, Cxs affect gene expression, migration, and other molecular mechanisms by acting in cytoplasm and nucleus, without forming hemichannels or gap junctions on the plasma membrane (Kotini et al., 2018).

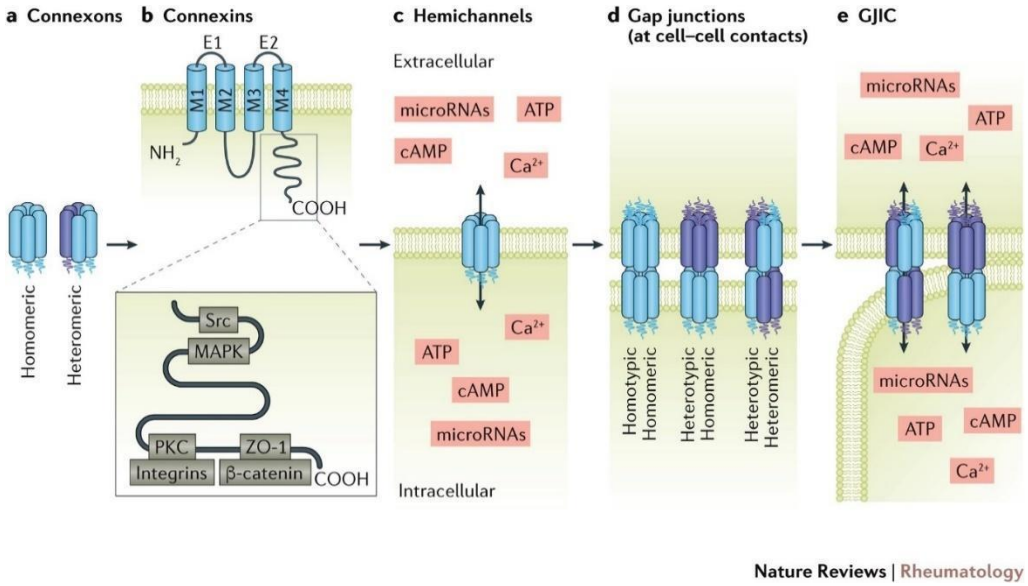

Figure 1.1. Schematic representation of connexins, hemichannels, and gap junctions (Donahue et al., 2018). (a) six single type Cx isoform or at least two Cx isoforms combine to form hemichannels called homomeric or heteromeric connexon/hemichannels, respectively. (b). Hemichannels can function alone on the cell membrane (c) or they dock with connexons of the same or different types on the cell membrane and make homotypic or heterotypic gap junction channels (d) to provide intercellular communication (e). M1-M4-transmembrane regions; E1-E2: extracellular loops; GJIC: gap junctional intercellular communication- intercellular communication with gap junctions.

Cx hemichannels and gap junctions are open and close according to the presence of the stimuli. The gating mechanism of Cx hemichannels and gap junctions are regulated by pH, post-translational modifications (PTMs), voltage and Ca^{2+}. In addition, each Cx hemichannel subunit indicates selective permeability to different substances such as Cx32 and Cx43 are more anion selective while Cx45 and Cx26 are more cation selective (Weber et al., 2004). It has been shown that Ca^{2+} has binding sites on extracellular side of the Cx hemichannels, such as D50 and K61 residues. These residues form salt-bridges to preserve pore lumen of the Cx hemichannels in resting phase. In the case of Ca^{2+} binding, these salt-bridges break, and the pore lumen expands. Ca^{2+} senses these residue motifs within or exposed to the pore lumen. The breakage in this salt-bridge with Ca^{2+} binding facilitates the opening of Cx26 and Cx30 (Lopez et al., 2016). Cx hemichannels are also regulated by ionic currents and voltage gating. Voltage drive alterations in the shape of ion channels by changing the position of charged amino acids. The changing in position is linked to other structural changes that determine whether the channel pore is

open or closed (Bargiello et al., 2018). As with Ca^{2+}, PTMs also affect the activity, stability, and localization of the Cxs. Phosphorylation acts as a molecular switch in channels and regulates Cx related signaling pathways. S-nitrosylation, covalent binding of NO on cysteine residues of C domain affect the permeability of the Cx26, Cx43 and Cx37 channels (Aesen, T. 2018).

1.3 Calcium as a key regulator in skin physiology

Ca^{2+} regulates various aspects of cellular functions within keratinocytes. The distribution and dynamics of Ca^{2+} in the skin are pivotal in maintaining epidermal homeostasis. In the mammalian epidermis, there exists a distinct calcium gradient, characterized by low levels in the basal layer, a progressive increase in the stratum granulosum, and decline in the stratum corneum (Pani & Singh, 2008). This calcium gradient is vital for the processes of keratinocyte differentiation and the establishment of the epidermal permeability barrier (S. E. Lee & Lee, 2018). In addition to playing role in division, proliferation, and differentiation of keratinocytes, intracellular and extracellular Ca^{2+} also controls the regulation of signaling pathways and formation of desmosomes, adherens and tight junctions that connect keratinocyte to each other or to the basement membrane (Tu et al., 2012). Furthermore, Ca^{2+} has been found as regulator of Cx assembly through Ca^{2+} binding protein, calmodulin which has binding sites on Cxs C terminal (Ahmad et al., n.d.).

The epidermal differentiation starts with the migration of keratinocytes upward from basal layer where keratinocytes mainly proliferate, to spinosum (Figure 1.2) (Pease et al., n.d.). At basal layer, Ca^{2+} concentration is low, and keratin 5 and keratin 14, which regulates keratinocyte proliferation expression occurs (Alam et al., 2011). At spinosum, medium levels of Ca^{2+} concentration is observed; keratin profile switch to keratin 1 and keratin 10 which regulates keratinocyte differentiation, and involucrin and transglutaminase are expressed (Yamamoto et al., 2003). When keratinocytes progress upward, they also produce lamellar bodies (LB), profilaggrin and laricrin at granular layer. In addition, Ca^{2+} levels are the highest at this level. At corneum, with the help of profilaggrin and loricrin, denucleated keratinocytes or corneocytes are formed for cornified envelope. This envelope composed of cytoskeletal and barrier-related molecules, mentioned above (Furue, 2020).

The functional skin barrier is found particularly in the stratum corneum. The stratum corneum is composed of corneocytes which are the product of keratinocyte differentiation, and (LB). LB includes cholesterol and free fatty acids, basically key components of a barrier. Therefore, LB is a specialized organelle that plays a role in lipid, protein, or antimicrobial barriers. Its homeostasis and barrier permeability are regulated by both extracellular Ca^{2+} concentration and Ca^{2+} influx through Ca^{2+} channels of the upper epidermis. The epidermal differentiation is vertical from the basal layer to the stratum corneum. Keratinocytes proliferate in the basal layer and differentiate upwards through epidermal layers. In each layer, differentiation markers are expressed variably. Ca^{2+} acts during this differentiation process. (Vičanová et al., 1998; S. E. Lee & Lee, 2018). It has been shown that Ca^{2+} regulates keratinocyte-specific genes through activator protein 1 (AP-1) which is a transcription factor (TF) of differentiation markers such as involucrin, profilaggrin, transglutaminase and some other keratins in spinosum and granular layers (Ng et al., 2000). As an example of this mechanism, high levels of Ca^{2+} are required for the expression of profilaggrin, a terminal differentiation marker, while low Ca^{2+} content is enough for the expression of keratin 1 and keratin 10, differentiation markers in granular layer (Yuspa et al., 1989). In addition, Ca^{2+}-sensitive protein, protein kinase C (PKC) also negatively regulates the expression of keratinocyte differentiation markers such as involucrin in spinosum layer (Deucher et al., 2002). Besides extracellular Ca^{2+}, intracellular Ca^{2+} also plays a role in epidermal differentiation. Ca^{2+} sensing receptor (CaSR) is expressed in stratum granulosa and elevates the intracellular Ca^{2+} in response to increased extracellular Ca^{2+} levels in this layer. After sensing the rise in extracellular Ca^{2+}, it activates phospholipase C and eventually IP_3 which activates the release of Ca^{2+} from ER and Golgi Ca^{2+} stores (Tu et al., 2012).

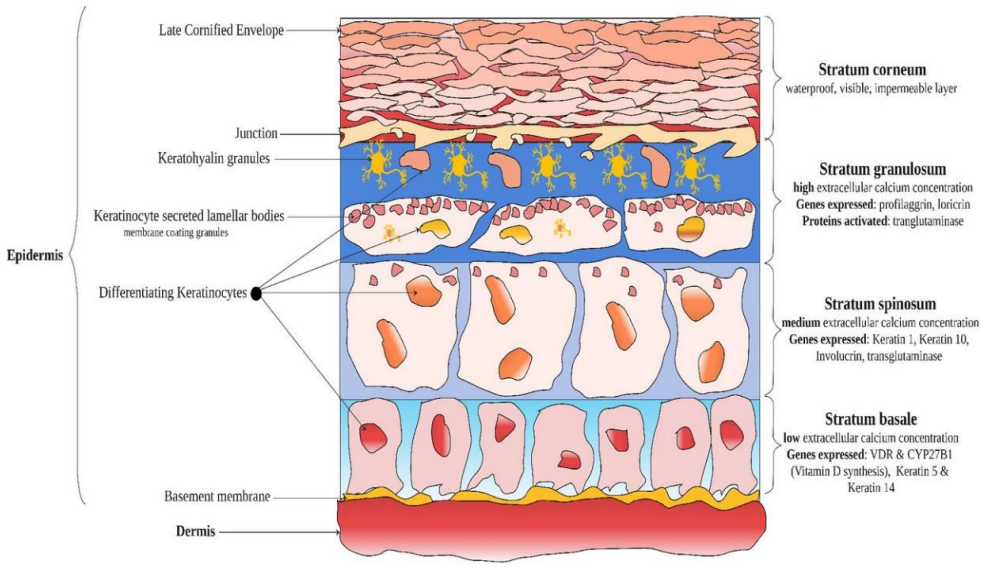

Figure 1.2. The epidermal layers, corneum, granolusum, spinosum and basal layers are represented with their gene expression profiles via Ca^{2+} gradient (Pease et al., 2022).

1.4 Connexin26 in Skin Abnormalities

Cx26 is one of the Cx types expressed in granular and spinosum layer, responsible for Ca^{2+} transport. Cx26 has multiple roles in skin, such as differentiation and proliferation by regulating the Ca^{2+} gradient between basal and granular layer (Scott et al., 2012). Mutations in the *GJB2* gene encoding Cx26 are common in humans. Even though most of the Cx26 mutations result with non-syndromic hearing loss, some Cx26 mutations also result in skin disorders. In normal physiological conditions, Cx26 open and close due to extracellular changes including differences in cation concentration, PTMs and voltage throughout the transmembrane. In pathological conditions such as microbe invasion or various connexin mutations, it has been observed that hemichannels can constantly open due to changes in the channel structures (Evans et al., 2006; Aypek et al., 2016). For example, during the invasion of epithelial cells by dysentery microbe, *Shigella* activates the Cx26 hemichannels and causes releasing of ATP to the outside and activating the calcium pathways in the cell. As a result, it has been observed that the bacteria increase the aggression and spread in the epithelial cells (Tran et al., 2003). Another study revealed that peptidoglycan (PGN) of commensal skin bacteria, *Staphylococcus epidermidis* and skin pathogen *Staphylococcus aureus* induced hemichannel activity in cells with Keratitis-Ichthyosis-Deafness (KID) syndrome mutations G12R and D66H, leading to the release of ATP (Donnelly et al., 2012).

It is known that mutations that cause Cx26, Cx30 and Cx43 proteins to form constantly open hemichannels induce hereditary diseases in humans (Essenfelder et al., 2004; Dobrowolski et al., 2007). It is thought that the formation of channels that work continuously in the cell membrane will cause uncontrolled transfer of molecules to the inside and outside, and this situation may adversely affect both the cell with the mutant channel and the neighboring cells metabolically and lead to pathologies seen in patients (Garcia-Vega et al., 2021). There are multiple skin disorders linked to mutations in Cxs. Even Cx26 deficiency did not show severe skin abnormalities compared to phenotypes of Cx43 and Cx30 deficiency, Cx26 mutations cause many different types of skin disorder (Ahmad et al., 2001; Sellitto et al., 2021).12 different types of Cx26 mutations linked to inherited skin disorders, such as Palmoplantar keratoderma with deafness (PPK), Vohwinkel syndrome (VS) and Keratitis-Ichthyosis-Deafness (KID) Syndrome (Srinivas et al., 2018). In PPK, Cx26 mutations lead to aberrant channel activity, resulting in abnormally thickened skin on the palms and soles, along with deafness (Lilly et al., 2016; Bedoukian et al., 2021). Likewise, in VS, Cx26 mutations cause aberrant channel activity and hemichannel docking, which in turn result in the formation of constricting bands around the fingers (pseudoainhum). These bands lead to the impairment of blood circulation to the digits and result in autoamputation. Additionally, individuals with VS exhibit thickened starfish-shaped patches on the top of their digits and knees, accompanied by sensorineural deafness (Bedoukian et al., 2021). KID Syndrome is also caused by 12 different types of mutations in Cx26, resulting with thickening of the skin in palms, soles, around eyes and inner ear (García et al., 2016).

1.5 Keratitis-Ichthyosis-Deafness (KID) Syndrome and Connexin26

Keratitis-Ichthyosis-Deafness (KID) syndrome is one of the genetic diseases caused by Cx26 mutations (Richard et al., 2002). KID syndrome is a rare autosomal dominant genetic disorder with thickening of the skin, keratitis, scaly skin, inflammation in cornea and deafness phenotypes. Severe cases of KID syndrome can be lethal due to dry skin and skin patches (Mese et al., 2011; García et al., 2016). Previous studies showed that Cx26 mutations in KID syndrome cause constantly open hemichannels and uncontrolled molecule (Ca^{2+}, cAMP, ATP) transfer between inside and outside of the cell resulting in the disruption of the cell homeostasis (Figure 1.1.a) (Evans et al., 2006; Srinivas et al., 2018). These Cx26 mutation types reveal variety in leaky hemichannels and severity of phenotypes. For example, G45E and A88V mutations are lethal in patients

due to inflammation while D50Y and I30N mutations reveal mild symptoms and hyperproliferation (Lopez et al., 2013; Lilly et al., 2016, 2019). In addition, Cx26 D50Y and I30N mutations showed an increase in Ca^{2+} concentration inside of the cell due to open hemichannels compared to N2A cells including Cx26 WT (Arndt et al., 2010.; Aypek et al., 2016). In a healthy epidermis, Cx26 expression is confined to the basal layer, establishing a Ca^{2+} gradient with peak levels in the granular layer and reduced levels in the basal layer (Figure 1.1.b). In KID syndrome-affected epidermis, the mutant Cx26 is widely expressed in all layers and abolishes the normal Ca^{2+} gradient (Figure 1.3.c). This loss of the Ca^{2+} gradient disrupts the typical regulation of keratinocyte proliferation (typically favored in low Ca^{2+}) and differentiation (typically favored in high Ca^{2+}), resulting in a significantly thickened epidermis and a decrease in differentiated cells. However, there is no direct evidence about the relationship between molecular mechanisms of disease phenotypes and Ca^{2+} homeostasis.

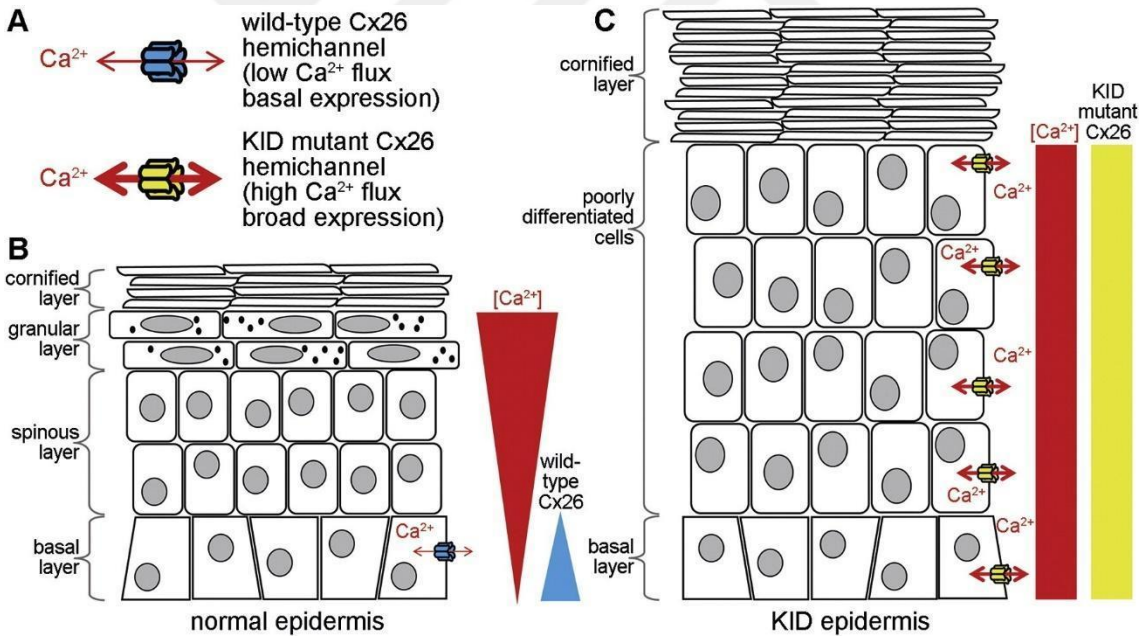

Figure 1.3. The effect of the disruption of the epidermal Ca^{2+} gradient by mutant Cx26 hemichannels in KID syndrome. (A) Mutant Cx26 KID hemichannels exhibit increased Ca^{2+} net flux and a broader expression pattern compared to wild-type. (B) Normal epidermis expressing Cx26 in the basal layer, establishing a Ca^{2+} gradient with peak levels in the granular layer and reduced levels in
Figure 1.3. (cont.) the basal layer. (C) In KID syndrome, the mutant Cx26 leads to widespread expression, intensifying Ca^{2+} flux, and abolishing the normal Ca^{2+} gradient (Srinavas, M. et al., 2018).

1.6 NF-κB signaling pathway

The nuclear factor kappa-light chain-enhancer of activated B cells (NF-κB) family is a group of transcription factors (TFs) that directly binds to DNA and induces gene expression when activated. These factors have important roles in development, innate and adaptive immune system, inflammation, cell proliferation, differentiation in almost all cell types and organogenesis of lymphoid organs in humans (Mitchell & Carmody, 2018). NF-κB TFs play equally significant roles in diseases where NF-κB activity is found to be disrupted. Therefore, they have critical pathological roles in inflammatory diseases. The NF-κB family is composed of five members which are p65 (RelA), RelB, c-Rel, p50 (active form of p105), and p52 (active form of p100). These factors usually work as homo or heterodimers and are found to be inactive in the cytoplasm. There are two main NF-κB signaling pathways, canonical and noncanonical (Figure 1.3). These pathways differ in the receptors for triggering activation of NF-κB proteins, the downstream intermediate elements, and the subsequently activated members of NF-κB family. In the canonical pathway, heterodimer of p50 and p65 is found as inactive in the cytoplasm bound to IκB∝ which masks the nuclear localization signals on conserved Rel homology domains (Oeckinghaus & Ghosh, 2009). When the signal comes to the canonical pathway receptors (e.g., TLRs, antigen receptors, cytokine receptors, growth factor receptors, stress) on the cell membrane, IKK complex (IKK-∝, IKK-β, and IKK-γ/NEMO) is activated by phosphorylation. The activated IKK complex then phosphorylates IκB that results in the release of NF-κB complex. The free NF-κB TF translocates to the nucleus and induces gene expression whereas the phosphorylated IκB is degraded by ubiquitination (Figure 1.3.a) (Zhang et al., 2017). In the noncanonical pathway, NF-κB activation depends on the NF-κB-inducing kinase (NIK) and IKK-∝ phosphorylation. The heterodimer p100/RelB is normally inactive and found in the cytoplasm similar to p50/p65 complex. p100 precursor dimerizes with RelB with its Rel homology domains and serve as a IκB with its carboxy-terminal ankyrin repeats (Oeckinghaus & Ghosh, 2009).When the signal activates the noncanonical pathway receptors on the cell membrane, p100 is phosphorylated and partially ubiquitinated to become active p52 protein. The free p52/RelB complex translocate to the nucleus and induces gene expression as shown in Figure 1.1 (Pflug & Sitcheran, 2020).

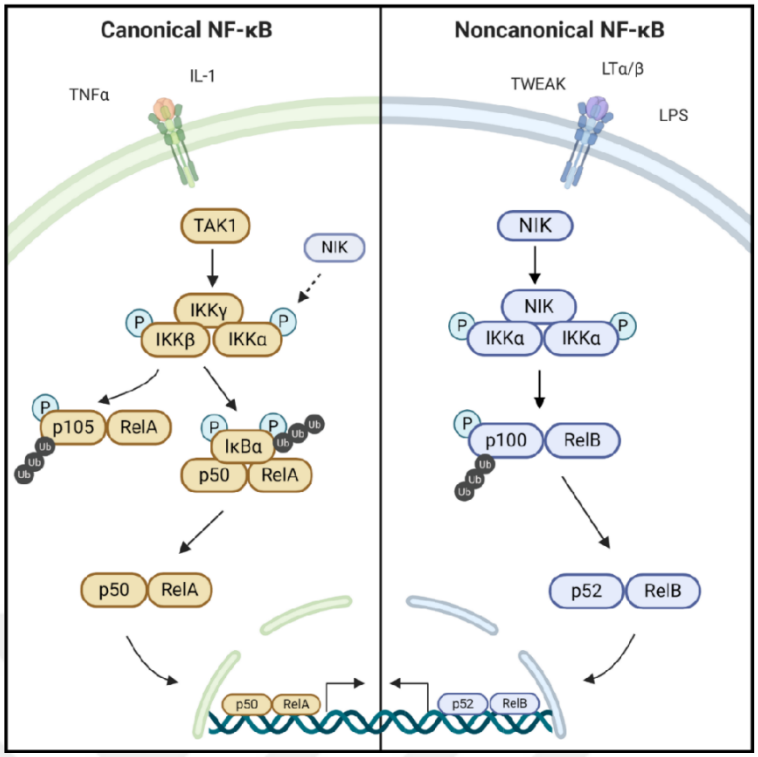

Figure 1.4. Comparison of canonical and non-canonical NF-κB signaling pathways (Pflug & Sitcheran, 2020).

1.6.1 The NF-κB pathway in skin physiology

The skin is composed of the epidermis and dermis. As mentioned above, the epidermis consists of proliferative and differentiative keratinocytes to form a skin barrier. The dermis is mainly composed of fibroblasts and immune cells accompanied by blood vessels, hair follicles, glands, and nerves. To function properly, a strong communication network among these various cell types is important for skin homeostasis. The skin immune cells such as macrophages and T cells are found in the dermis, and they are critical for host defense of the skin in response to external stimuli like pathogens (H. J. Lee & Kim, 2022). Besides immune cells, epidermal keratinocytes have been found as a key player in skin immune homeostasis. It has been shown that inflammation-related molecules such as the NF-κB pathway in the epidermis have a major role in the skin. Impaired regulation of the NF-κB pathway in both keratinocytes and T cells revealed inflammatory skin in IkB deficient mice models (Rebholz et al., 2007). In another study, IKK-β overexpressing mice showed thickened and inflammatory skin phenotypes. These phenotypes are also accompanied by increased expression of inflammatory cytokines and upregulated inflammatory genes (Page et al., 2010). In addition, p65/c-Rel deficient

epidermis revealed skin inflammation, suggesting p65 and c-Rel NF-κB TFs are essential for the maintenance of skin immune homeostasis (Gugasyan et al., 2004). This idea has been also proved by the study revealed that RelB deficiency developed skin inflammation (Weih et al., 1997). Overall, the epidermis regulates proinflammatory factors through the NF-κB pathway accompanied by immune cells to maintain immune homeostasis of the skin (Wullaert et al., 2011).

In addition to its role in maintaining skin immune homeostasis, NF-κB has been identified as a crucial regulator of epidermal development and homeostasis (Figure 1.5). NF-κB subunits, including p65, p50, RelB, and c-Rel, have been observed to predominantly localize in the cytoplasm of basal layer, where their activation influences differentiation and inhibits proliferation (Weih et al., 1997; Gugasyan et al., 2004). Furthermore, it has been noted that a high concentration of Ca^{2+} inhibits keratinocyte proliferation (Takao, 2003). NF-κB subunits exert their regulatory effects by modulating cell cycle dynamics. Specifically, downregulation of c-Rel has been associated with increased apoptosis and decreased keratinocyte proliferation, leading to a G_2/M state delay due to the upregulation of its regulatory proteins (Lorenz et al., 2014). Additionally, the knockout of IKK-α in mice has resulted in atypical differentiation characterized by upregulated early differentiation markers, K14 and K10, and downregulated late differentiation markers, such as filaggrin (Q. Li et al., 1999). Similarly, the overexpression of p65, p50, or c-Rel has been found to inhibit cell growth and promote terminal differentiation (Seitz et al., 2000). Conversely, mice lacking p65 and c-Rel exhibited reduced epidermal growth and proliferation. Another study demonstrated that p65 and c-Rel deficient mice developed tumor necrosis factor-alpha (TNF-α)-dependent hyperproliferation in their skin, accompanied by a reduction in late differentiation markers K14 and K10 (Gugasyan et al., 2004; Grinberg-Bleyer et al., 2015). Furthermore, IKK-α has been identified as vital for keratinocytes to proliferate and differentiate by preventing apoptosis induced by TNF-α (Hu et al., 2001). In addition, IKK-γ-deficient mice displayed abnormal skin characterized by hyperproliferation, hyperkeratosis, and inflammation (Makris, 2000).

The regulation of NF-κB pathway in skin is dependent in numerous factors. Upstream regulators of NF-κB pathway was found as caspase recruitment domain 10 (CARD10) and CARD14, which facilitates keratinocyte proliferation. It has been shown that CARD14 deficiency increased NF-κB activation and caused atopic dermatitis (Peled

et al., 2019). Likewise, TNF-α deficiency increased IKK activity (Makris, 2000). Another regulator, receptor interacting serine-threonine kinase (RIPK4) interacted with PKC and regulated keratinocyte differentiation by mediating the activation of NF-κB (Bahr et al., 2000). The NF-κB pathway also regulates its own activation. It has been found that p65 deficiency caused decreased expression of c-Rel and RelB. In addition, p65 was required for developing skin tumorigenesis where Birc3, an anti-apoptotic gene was downregulated in p65 deficiency, which explained p65 promoted tumorigenesis in skin (Kim & Pasparakis, 2014). In normal conditions, p65 induced cell survival. The study showed that cell cycle was arrested by activated p21 through TNF-α induced NF-κB activation in keratinocytes (Basile et al., 2003).

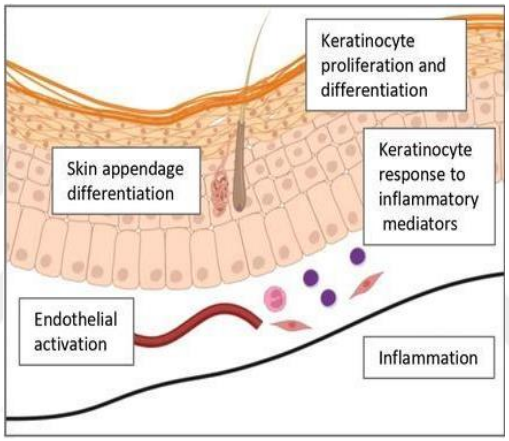

Figure 1.5. Summary of skin homeostasis regulated by NF-κB Pathway (Adapted from: Shen, Y 2023)

1.6.2 The relation between Ca^{2+} and NF-κB pathway

The regulation of epidermal homeostasis is maintained by both Ca^{2+} and the NF-κB pathway, as previously discussed. Studies have demonstrated that Ca^{2+} exerts a positive regulatory effect on differentiation by activating differentiation markers (Al-Ani et al., 1988). Similarly, the NF-κB pathway also regulates similar differentiation markers (Gugasyan et al., 2004). Ca^{2+} plays a role in various physiological processes, including cell survival/death through Calcineurin and PKC, cell homeostasis through ER-Ca^{2+} channels like SERCA pumps, endo/exocytosis through S100 proteins, and gene expression through Calmodulin (CaM). Among these, CaM is a major Ca^{2+}-binding protein that facilitates all of these cellular events (Bagur & Hajnóczky, 2017). Research has shown that under normal extracellular Ca^{2+} levels, keratinocytes undergo rapid division,

and CaM expression is upregulated. Conversely, low levels of extracellular Ca^{2+} result in opposite phenotypes (Al-Ani et al., 1988). Similarly, Ca^{2+}/CaM is required for keratinocyte differentiation (Mahanty et al., 2019).

Moreover, CaM has been found to interact with NF-κB activation in the skin. A study revealed that Ca^{2+}/CaM-dependent protein kinase 4 (CaMK4) regulates the expression of IL-17, which is upregulated in immune-mediated skin disorders such as psoriasis. CaMK4 promotes inflammation in keratinocytes through the AKT-NF-κB pathways. CaMK4 deficiency leads to decreased levels of skin pathogenic factors like S100 and TNF, increased apoptosis, and decreased cell proliferation. Additionally, CaMK4 downregulation reduces the phosphorylation of AKT, IKK-α, IKK-β, and p65(Yong et al., 2022).

The relationship between Ca^{2+} and the NF-κB pathway has been documented in several studies conducted in different cell types. In human epidermoid squamous cell carcinoma cells (A-431), NF-κB (p65 and c-Rel) was found to be upregulated through epidermal growth factor (EGF). However, this activation was impaired by the introduction of the intracellular Ca^{2+} chelator, BAPTA-AM (Sun & Carpenter, 1998). Furthermore, it has been demonstrated that CaM binds to both p65 and c-Rel after their release from IκB, inhibiting the nuclear translocation of c-Rel while having no effect on the nuclear translocation of p65(Antonsson et al., 2003). In addition, in lymphocytes, the link between Ca^{2+} and the NF-κB pathway was proved several times.

1.7 Aim of the Study

As a result of proteomic pre-studies, IKK-γ/NEMO, which positively regulates NF-κB signaling, was found only in Cx26-D50Y expressing keratinocytes. For this reason, it is hypothesized that the NF-κB pathway might be activated in keratinocytes expressing the leaky Cx26 hemichannel resulting from the D50Y mutation. It is hypothesized that this pathway might cause the epidermis to differentiate more than normal by changing the proliferation and/or differentiation mechanisms of keratinocytes. The IKK-γ mutations cause “anhidrotic ectodermal dysplasia with immune deficiency” which results with problems in tissues such as skin, hair and sweat glands that develop from the ectoderm in humans (Keller et al., 2011). Also, IKK-γ deficient mice displayed abnormal skin characterized by hyperproliferation (Makris, 2000). The similarity of epidermal abnormalities (keratinocyte differentiation/proliferation disorders and over-

thickness of epidermis) observed in human epidermal disorders caused by IKK-γ mutations and in NF-κB knockout mouse models with the phenotypes of KID syndrome mouse model, strengthen the hypothesis that suggests Cx26 mutations are likely to lead to disrupted Ca^{2+} homeostasis, subsequently impairing the regulation of the NF-κB signaling pathway (Mese et al., 2011; García et al., 2016). The positive correlation between Ca^{2+} and NF-κB pathway on epidermal differentiation processes also supported this idea. It has been shown that KID Syndrome Cx26-G45E and Cx26-D50Y mutations both revealed Ca^{2+} leakage but resulted with different phenotypes; lethality and hyperkeratosis, respectively (García et al., 2016). Based on the hypothesis, it is aimed to investigate the effects of the Ca^{2+} on NF-κB signaling pathway in keratinocytes that permanently express Cx26-D50Y and Cx26-G45E mutations, which cause different severity in patients. Hereby, suitability of targeting NF-κB signaling pathway either in the treatment of patients with KID syndrome or reducing symptoms will also be investigated.

CHAPTER 2

MATERIALS AND METHODS

2.1 Maintenance of HaCaT Cells

Human keratinocyte cells (HaCaT) were used. HaCaT cells were grown in high glucose Dulbecco's Modified Eagle Medium (DMEM, GIBCO, Cat# 41966029) medium. DMEM medium was supplemented with 10% Fetal Bovine Serum (FBS, GIBCO, Cat# 16000044) and 1% Penicillin/Streptomycin (P/S, GIBCO, Cat # 15140122). The cells were incubated at 37°C in the incubator which was humidified with 5% CO_2. HaCaT cells were infected with MSCV retroviral vector including Cx26-WT, Cx26-G45E and Cx26-D50Y cDNAs. The cell groups infected with MSCV-Cx26-WT was referred as WT, MSCV-Cx26-G45E as G45E and MSCV-Cx26-D50Y as D50Y, respectively throughout the thesis. Empty MSCV vector was used as control and referred as MSCV. 3.2 mM $CaCl_2$ was added to the infected HaCaT cells' medium to keep hemichannels constantly closed and support cell growth.

HaCaT cells were passaged in their log phase by incubating them first with 0.05% EDTA (Biological Industries, Cat# 03-015-1B) for 20 minutes and then with 0..25 % Trypsin EDTA (Biological Industries, Cat# 03-053-1A) for 5 minutes at 37˚C and 5% CO_2 humidified atmosphere.

2.2 Trypan Blue Staining for Cell Counting

For 10 cm dish, $1.2x10^5$; 6 cm dish, $4.0x10^4$; 6 well plate, $2.0x10^4$ and 12 well plate, $0.5x10^4$ HaCaT cells were used. After trypsinization, cells were centrifuged and resuspended in 1 ml DMEM medium including 3.2 mM $CaCl_2$. Then, 10 µl cell mixture was added into 50 µl trypan blue dye diluted in 140 µl DMEM medium followed by taking 10 µl dye-cell mixture and loading onto the haemocytometer. Average number of cells were calculated and cell amount in 1000 µl solution was obtained by multiplying with the dilution factors.

2.3 Western Blot Analysis

2.3.1 Cell Lysis for Total Protein

$4.0x10^4$ cells were seeded into 6 cm dishes in 5 ml medium/ dish and cultured for 48 hours for 80-90% confluency. Then, cells were rinsed with 0.05% EDTA for 20 minutes. After cells were trypsinized, they were centrifuged for 2 minutes at 3,000 rpm. The supernatants were aspirated, and 1000 µl 0.05% EDTA was added to each cell pellet without resuspending. 0.05% EDTA were aspirated after 3,000 rpm centrifugation for 1 minute. Cell pellets were then resuspended with 100 µl lysis buffer (100 mM Tris-HCl, 1mM EDTA, 0.1% Triton X). After the cells were homogenized with 26G 1 ml insulin syringes, they were kept on ice for 15 minutes. After a short vortex, the cells were centrifuged at 14,000 rpm for 20 minutes at +4°C. Then supernatants were taken into Eppendorf tubes and saved for Bradford analysis. For long time storage, total protein samples were put into -80°C.

2.3.2 Bradford Assay

Bradford assay consisted of two steps. In the first step, BSA (20 mg/ml) standards were prepared as 0.25 mg/ml, 0.5 mg/ml, 1 mg/ml, 2 mg/ml, and 4 mg/ml. 800 µl autoclaved dH_2O and 200 µl 5X Bradford reagent was mixed into cuvettes to obtain 1X Bradford reagent. 10 µl BSA standards were added into each 1X Bradford reagent to obtain a standard curve. In the second step, the same dilutions of Bradford reagent were prepared for total protein samples as well. 10 µl of protein samples after heating at 95 °C for 5 minutes, were loaded into 1X Bradford solution. Concentration of proteins were measured at 595 nm on spectrometer and each protein sample was standardized based on the protein sample that had the lowest concentration.

2.3.3 Immunoblotting

SDS-PAGE resolving gels were prepared in 12% concentration with 5% stacking gels for analysis of total protein samples. After protein concentrations were set, 5X loading buffer that was also heated at 95°C for 5 minutes with protein samples, was added onto the samples. Then, 15 µl samples and 1 µl Color Prestained Protein Standard (NEB, Cat# P7719S) were loaded into the gel and run at 40V minutes for 1.5 hour, 60V for 15 minutes and 90V for 30 minutes. After the protein samples were resolved in SDS PAGE, they were transferred to the PVDF membrane at 90V for 2 hours in ice cold temperature.

Membranes were blocked with 3% Bovine Serum Albumin (BSA)-1X Tris Buffer Saline-Tween 20 (TBS-T) solution for 1.5 hours at room temperature at 60 rpm. Membranes were incubated with primary antibody against p65 (1:1000; SantaCruz, Cat# sc-8008), p-p65 (1:1000; SantaCruz, Cat# sc-136548), RelB (1:1000; SantaCruz, Cat# sc-48366), c-Rel (1:1000; Cell Signaling Technology, Cat# E8Z5Y), IKK-γ (1:1000; SantaCruz, Cat# sc-8032), Connexin26 (1:1000; Invitrogen, Cat# 710500), γ-tubulin (1:1000; Sigma, Cat# T65557) and β-actin (1:1000; Abcam, Cat# ab8227) at 4°Cover night. The following day, the membranes were rinsed with 1X TBS-T solution three times for 10 minutes. Then, membranes were incubated with anti-rabbit (1:1000; ThermoScientific, Cat# 31460) or anti-mouse (1:1000; DAKO, Cat# P0447) secondary antibodies for 2 hours at 60 rpm rocker at room temperature. In these experiments, γ-tubulin and β-actin were used as loading controls, and the same membrane was used for the quantification of γ-Tubulin or β-actin following the same protocol. After rinsing the membranes three times for 10 minutes with 1X TBS-T, chemiluminescence (BIORAD, 1705061) was applied and the membrane was visualized with the FUSION SL VILBER LOURMAT imaging system.

2.4 q-RT PCR Analysis

Primers designed for use in molecular expression analysis (Table 2.2) were dissolved in nuclease-free water, and the final solution was obtained by diluting the 500X stock solution to 10X. For total RNA isolation, $2.0x10^4$ MSCV, WT, G45E and D50Y cells were seeded into 6-well plates in 2ml medium/ well. After 48 hours incubation, cells were washed with cold 1X PBS and flash frozen with liquid nitrogen. The total RNA isolation was performed by following the Monarch® Total RNA Miniprep Kit (Cat# T2010S) protocol. The RNA concentrations of the obtained samples were measured using Nano-drop. The cDNAs obtained from 1µg RNA with the Revertaid 1St cDNA Synthesis Kit (ThermoScientific, Cat# K1622) were used for q-RT-PCR analysis. Then, cDNA samples were used for amplification with q-RT-PCR (Roche LightCycler® 96 system) with RealQ Plus 2x Green Master Mix (Ampliqon, Cat# APQ-A323402). After the amplification process, cycle time (Ct) values of gene of interests were normalized to the Ct value of Tata-Box Binding Protein (TBP) and fold changes were calculated with the Delta Ct formula, $2^{-\Delta\Delta Ct} = 2^{\text{control group (target gene Ct value- TBP Ct value)-experimental group (target gene Ct value- TBP Ct value)}}$. The used cycle and primer sequences are shown in Table 2.1 and Table 2.2, respectively.

Table 2.1 Cycles used in q-RT PCR.

Stage	Temperature	Duration	Cycle
Preincubation	95°C	900 s	1 cycle
	95°C	30 s	45 cycle
3 step amplification	60°C		
	72°C		
	95°C	10 s	1 cycle
Melting	65°C	60 s	
	72°C	1 s	

Table 2.2. Forward and Reverse Primers of genes amplified in q-RT PCR.

Gene Name	Forward Primer	Reverse Primer
Human TBP	5'-tagaaggccttgtgctcacc-3'	5'-tctgctctgactttagcacct-3'
P65	5'-gcacagataccaccaagacc-3'	5'-tcagcctcatagaagccatc-3'
RelB	5'-agattgaggctgccattgag-3'	5'-cgcagctctgatgtgtttgt-3'
c-Rel	5'-aggggaatgcgttttagat-3'	5'-ccgtctctgcagtcttttcc-3'
IKK-γ	5'-agctgcagagggagtacagc-3'	5'-tctgcagggtgtccatatca-3'
Connexin26	5'-ctgcagctgatc-3'	5'-aagcagtccaca-3'

2.5 BAPTA and BAPTA-AM treatment

Optimization experiments of BAPTA (Cayman, Cat# 11706) and BAPTA-AM (Tocris, Cat# 2787) chemicals were performed. 1 μM, 2.5 μM and 5 μM BAPTA-AM and 10 μM, 25 μM and 50 μM BAPTA chemicals were prepared by dissolving in DMSO and optimized with staining with 5 μM Fluo-3AM (Invitrogen, Cat# F14218) Ca^{2+} dye for 6, 12 and 24 hours. Fluo-3 AM dye was added to the medium every 6 hours. Control experiments were carried out by using DMSO in corresponding volumes of BAPTA and BAPTA-AM and incubated for 12 hours. $2.0x10^4$ cells MSCV, WT, G45E and D50Y cells were seeded into the 6-well plate in 2ml medium/ well and incubated for 48 hours. Each chemical concentration and incubation time optimization experiment consisted of three samples and each sample consisted of three replicates.

All BAPTA-AM and BAPTA experiments were conducted by treating cells seeded for total protein, total RNA samples, Dual-Luciferase Reporter assay, or immunofluorescence with BAPTA-AM or BAPTA with their corresponding DMSO controls for 6 hours just before the experiments.

2.5 Dual-Luciferase Reporter Assay

$0.5x10^4$ HaCaT MSCV, WT, G45E and D50Y cells were seeded into the 12-well plate in 1 ml medium/well. After 12 hours incubation, cells were transfected with the plasmids, ConA luciferase control and ConB NF-κB luciferase, kindly provided by Prof. Neil Perkins (University of Glasgow; (Campbell et al., 2006) using FuGENE® HD Transfection Reagent (Promega, Cat# E2311) by following the manufacturer's protocol. After 12 hours incubation, Luciferase Reporter Assay was conducted by following the manufacturer's protocol of Dual-Luciferase Reporter Assay Kit (Promega, Cat# E1910). Samples were taken into 96 well plate and luminometric measurements were conducted by Thermo Scientific Varioskan® Flash.

2.6 Immunostaining and Fluorescence Microscopy Analysis

$2.0x10^4$ HaCaT MSCV, WT, G45E and D50Y cells were seeded on coverslips in 6 well plates and cultured for 48 hours. After the incubation, cells were rinsed with 1 ml 1X Phosphate Buffered Saline (PBS) for three times and then were permeabilized with 0.1 % TritonX-100/PBS at room temperature for 15 minutes. Next, permeabilized cells were blocked in 5 % BSA in 0.1 % TritonX-100/PBS at room temperature for 45 minutes to inhibit non-specific binding. Then, cells were stained with polyclonal mouse anti-p65 (1:200; SantaCruz, Cat# sc-8008), polyclonal mouse anti-RelB (1:200; SantaCruz, Cat# sc-48366), monoclonal rabbit anti-c-Rel (1:200; Cell Signaling Technology, Cat# E8Z5Y), at +4°C overnight. After incubation, cells were rinsed with 1X PBS three times to remove non-specific bindings and incubated with Alexa555-conjugated goat anti-rabbit secondary antibody (1:200; Invitrogen, Cat# A21428) or Alexa555-conjugated goat anti-mouse secondary antibody (1:200; Invitrogen, Cat# A21427), phalloidin (1:300; Invitrogen, Cat# A12379) and DAPI (1:1000; Sigma, Cat #D9542) for 45 minutes at room temperature in dark conditions. After the rinsing of cells with 1X PBS for three times, coverslips were dipped into dH_2O and mounted onto the slides.

Then, images were taken by Olympus ix83 fluorescent microscope and analysed using ImageJ program.

2.7 Statistical Analysis

All experiments were performed in triplicates (otherwise it was mentioned) and results were reported as mean± standard deviation. Differences between MSCV and WT, G45E or D50Y cells were statistically assessed by unpaired t-test. n represents the total sample size in each experiment and p values are detailed in each figure legend with its statistical significance.

CHAPTER 2

RESULTS

3.1 SECTION I

3.1.1. Connexin26 overexpression was verified in HaCaT cells expression Cx26-WT while Cx26 KID Syndrome mutations revealed opposite pattern of Cx26 expression.

To address the functional significance of Cx26 overexpression and mutations on keratinocytes, Cx26 WT, G45E and D50Y expressions were selectively ensured with MSCV-Cx26-WT-GFP, MSCV-Cx26-G45E-GFP, and MSCV-Cx26-D50Y-GFP constructs. HaCaT cells with each construct were analyzed by Western Blotting and q-RT-PCR using specific antibodies and primers against Cx26, respectively. γ-tubulin or β-actin were used as a loading control and Cx26 protein levels were normalized to γ-Tubulin or β-actin. Similarly, TBP was used as a housekeeping gene and Cx26 mRNA levels were normalized to TBP in q-RT-PCR analysis. Fold differences were assessed in HaCaT cells expressing each construct by normalization of their protein or mRNA levels to control cells infected with MSCV-GFP. Overall results were shown in Table 4.1.

According to results below, Cx26 protein levels increased by 75% in D50Y compared to WT but G45E showed a slight decrease (18%) in Cx26 protein levels (Figure 3.1.1.A: n=3). Similarly, Cx26 mRNA expression was approximately 5-fold increase in WT and D50Y, decreased by 10% in G45E with respect to MSCV. Compared to WT, D50Y revealed slightly more expression of Cx26 and G45E had 80% decreased expression of Cx26 (Figure 3.1.1.B.; n= 6).

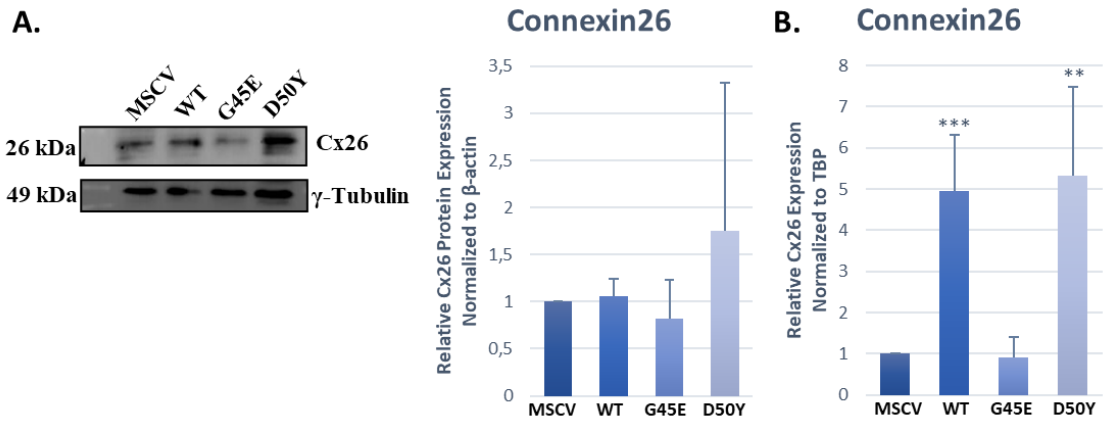

Figure 3.1.1 Connexin26 expression levels for MSCV, WT, G45E and D50Y. (A) Relative Cx26 protein expression level for WT, G45E and D50Y cells with respect to control MSCV cells (n= 3, ns) (B) Relative Cx26 mRNA expression level for WT, G45E and D50Y cells with respect to control MSCV cells (n=6, ** $p<0.01$; *** $p<0.005$). Statistical significance was assessed by unpaired t test (** $p<0.01$; *** $p<0.005$). The error bars represent the standard deviation.

3.1.2. Cx26 overexpression and Cx26 KID Syndrome mutations affected the NF-κB activation.

The proteomic studies revealed that D50Y showed increased NF-κB pathway component expression as mentioned above. To determine how Cx26 overexpression and Cx26 KID syndrome mutations affect NF-κB gene expression, Dual-Luciferase Reporter assay was applied to test the activation of canonical NF-κB pathway. The differences were assessed by normalization to control MSCV cells. Similar to Cx26 expression pattern among cells, NF-κB activation increased by 50% in WT and approximately 2.5-fold in D50Y while decreased by 72% in G45E compared to controls. Compared to WT, NF-κB activity increased by 53% in D50Y while decreased by 86% in G45E (Figure 3.1.2; n=4). Together with the previous results, D50Y KID syndrome mutation showed a significant increase while G45E showed reduced activation of NF-κB.

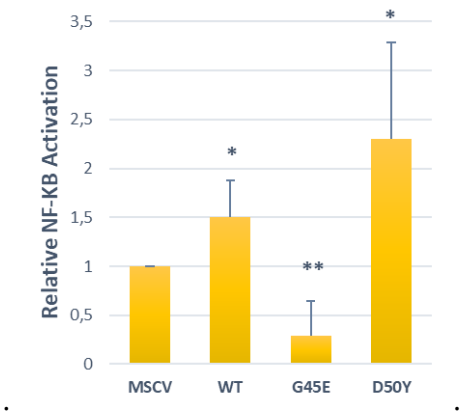

Figure 3.1.2 Relative NF-κB expression levels for WT, G45E and D50Y with respect to MSCV control cells (n=4, * p<0.05; ** p<0.01). Statistical significance was assessed by unpaired t test (* p<0.05; ** p<0.01). The error bars represent the standard deviation.

3.1.3. Cx26 overexpression and Cx26 KID Syndrome mutations affected the expression pattern and activation of canonical NF-κB transcription factors.

The impact of Cx26 overexpression and Cx26 KID syndrome mutations on canonical NF-κB pathway molecules was assessed by Western blotting and q-RT-PCR using specific antibodies and primers against p65, p-p65, c-Rel and IKK-γ, respectively. Fold differences were normalized to MSCV control cells. p65 protein levels decreased by 34% in WT (Figure 3.1.3.A; n=3), while G45 and D50Y did not indicate significant change (Figure 3.1.3.A; n=3, ns). Compared to WT, p65 protein level did not change in G45E and D50Y. Similar to protein level, p65 mRNA levels decreased by approximately 20% in WT and D50Y (Figure 3.1.3.B; n=6) while G45E did not indicate a significant change (Figure 3.1.3.B; n=6, ns). In both p65 protein and mRNA levels, G45E had higher p65 expression compared to WT.

The activated p65 protein is phosphorylated p65 protein (p-p65) and fold differences was normalized to total p65 protein levels of each HaCaT cells expressing WT, G45E and D50Y construct. Then, all results were normalized to control MSCV cells. WT and G45 cells indicated a significant increase by 2.3-fold and 44% in p-p65 levels, respectively (Figure 3.1.3.C; n=4). On the other hand, D50Y did not show any significant change in p-p65 protein levels (Figure 3.1.3.C; n=4). In contrast to p65, p-p65 showed less expression in G45E and D50Y compared to WT.

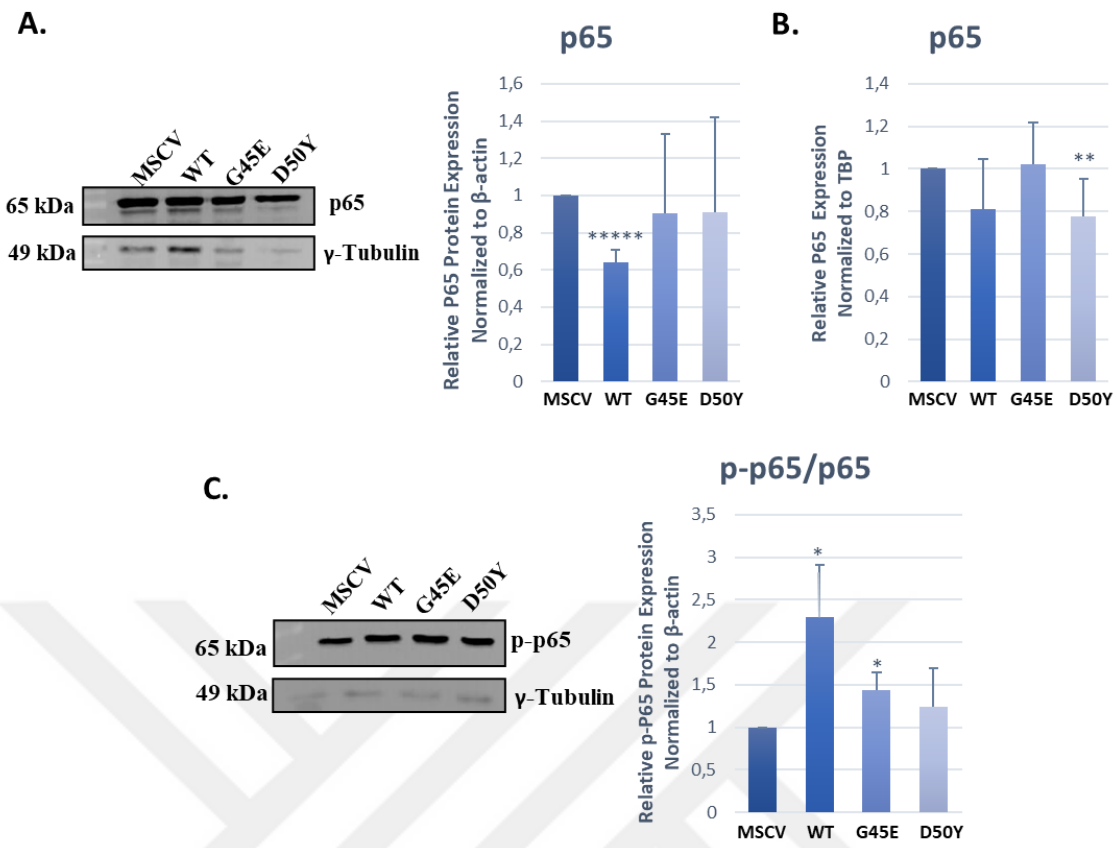

Figure 3.1.3. p65 expression levels for MSCV, WT, G45E and D50Y. (A) Relative p65 protein expression level for WT, G45E and D50Y cells with respect to control MSCV cells (n=4 , ***** p< 0.0001) (B) Relative p65 mRNA expression level for WT, G45E and D50Y cells with respect to control MSCV cells (n=6, ** p<0.01) (C) Relative p65 activation levels (p-p65 compared to p65 protein expression levels) for WT, G45E and D50Y cells with respect to control MSCV cells (n=4, * p< 0.05). Statistical significance was assessed by unpaired t test (* p<0.05; ** p<0.01; ***** p< 0.0001). The error bars represent the standard deviation.

Another canonical NF-κB pathway member is c-Rel. In Western Blotting results, G45E indicated 19% increase (Figure 3.1.4.A; n=4) while WT and D50Y did not show any significant change. Similarly, c-Rel mRNA expression increased by 23% in G45E and decreased by 33% in D50Y (Figure 3.1.4.B; n=4). Compared to WT cells, G45E had approximately 20% higher and D50Y had approximately 30% less c-Rel expression. However, WT did not reveal any significant change in c-Rel mRNA expression (Figure 3.1.4.B; n=6).

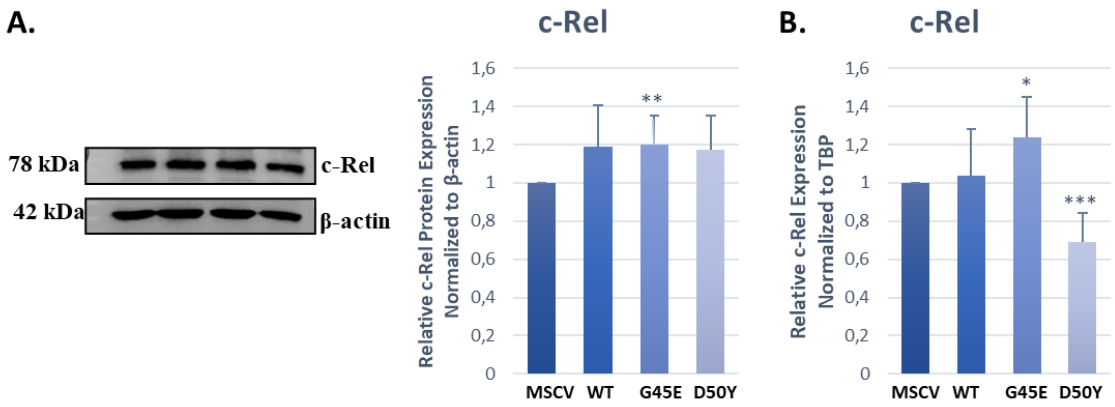

Figure 3.1.4. c-Rel expression levels for MSCV, WT, G45E and D50Y. (A) Relative c-Rel protein expression level for WT, G45E and D50Y cells with respect to control MSCV cells (n=4, ** p< 0.01) (B) Relative c-Rel mRNA expression level for WT, G45E and D50Y cells with respect to control MSCV cells (n= 6, * p<0.05; *** p<0.0001). Statistical significance was assessed by unpaired t test (* p<0.05; ** p<0.01; *** p<0.005). The error bars represent the standard deviation.

Another key factor of NF-κB pathway, IKK-γ was also analyzed by Western Blotting and q-RT-PCR (Figure 3.1.5). IKK-γ protein levels dropped by 25% in G45E (Figure 3.1.5.A; n=3) while WT and D50Y cells did not show any significant change (Figure 3.1.5.A; n=3). IKK-γ mRNA expression reduced by 40% in D50Y (Figure 3.1.5.B; n=6) while WT and G45E cells did not show any significant change (Figure 3.1.5.B; n=6). Compared to WT, IKK-γ protein levels dropped in G45E and mRNA expression decreased in D50Y.

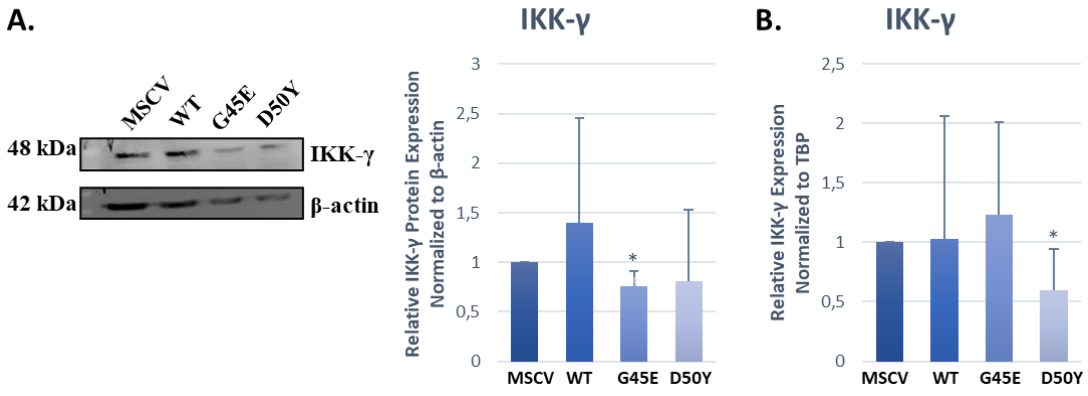

Figure 3.1.5. IKK-γ expression levels for MSCV, WT, G45E and D50Y. (A) Relative IKK-γ protein expression level for WT, G45E and D50Y cells with respect to control MSCV cells (n=3, * p< 0.05) (B) Relative IKK-γ mRNA expression level for WT, G45E and D50Y cells with respect to control MSCV cells (n=6, * p<0.05). Statistical significance was assessed by unpaired t test (* p<0.05). The error bars represent the standard deviation.

Overall, NF-κB pathway members revealed different expression patterns among experimental groups. p65 expression similarly dropped in WT and D50Y while p-p65 expression was high in WT Cx26 overexpression group. c-Rel expression was high in G45E compared to WT. p65, c-Rel and IKK-γ indicated low mRNA expression in D50Y.

3.1.4. Cx26 overexpression and Cx26 KID Syndrome mutations decreased the expression of non-canonical NF-κB transcription factor.

The impact of Cx26 overexpression and Cx26 KID syndrome mutations on noncanonical NF-κB pathway was also assessed by Western Blotting and q-RT-PCR using specific antibodies and primers against RelB. Fold differences were normalized to MSCV. Based on the results (Figure 3.1.6), RelB protein levels declined by 19% and 64% in WT and D50Y, respectively (Figure 3.1.6.A; n=3). G45E did not indicate a significant change in RelB protein levels ((Figure 3.1.6.A; n= 3). D50Y showed 55% decrease in RelB protein levels compared to WT. Similarly, RelB mRNA levels dropped by 12% in WT, 15% in G45E and 58% in D50Y (Figure 3.1.6.B; n=6). Further, compared to WT, RelB expression was slightly decreased in G45E and decreased by half in D50Y.

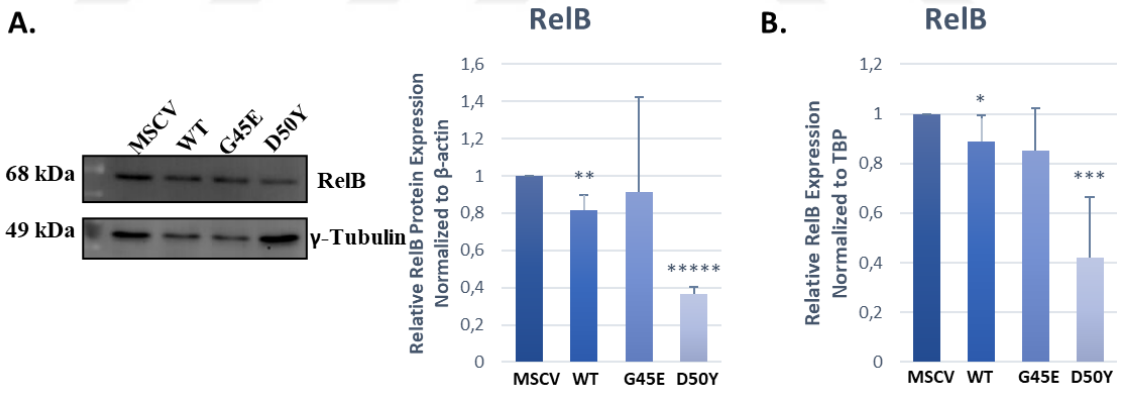

Figure 3.1.6. RelB expression levels for MSCV, WT, G45E and D50Y. (A) Relative RelB protein expression level for WT, G45E and D50Y cells with respect to control MSCV cells (n=3, ** p< 0.01; ***** p< 0.0001) (B) Relative RelB mRNA expression level for WT, G45E and D50Y cells with respect to control MSCV cells (n=6, ± p<0.1; * p<0.05; *** p<0.005). Statistical significance was assessed by unpaired t test (* p<0.05; ** p<0.01; *** p<0.005; ***** p< 0.0001). The error bars represent the standard deviation.

3.2 SECTION II

3.2.1 Verification of the reduction of intracellular and extracellular Ca^{2+} in HaCaT cells expressing Cx26-G45E construct.

Ca^{2+} was mentioned as a key regulator of epidermal homeostasis and its transport was facilitated by Cxs (REFERENCE). To examine the impact of Ca^{2+} on NF-κB pathway, both intracellular and extracellular Ca^{2+} levels were modulated by BAPTA-AM and BAPTA, respectively. A calcium dye, Fluo-3AM was used to verify BAPTA-AM and BAPTA activity. Optimization assays were done with HaCaT cells expressing Cx26-G45E-GFP construct which form constitutively active hemichannels that resulted in increased Ca^{2+} levels in cells to better understanding changes in Ca^{2+} signal levels. The optimization results were shown in Figure 3.2.1. As controls, corresponding volumes of DMSO were used. G45E cells treated with 25 µM BAPTA indicated a noticeable decrease in Fluo-3AM Ca^{2+} signals (Figure 3.2.1.A). G45E cells treated with 5 µM BAPTA-AM indicated a noticeable decrease in Fluo-3AM Ca^{2+} signals (Figure 3.2.1.B). As a result, following experiments were conducted with 25 µM BAPTA and 5 µM BAPTA-AM treatments.

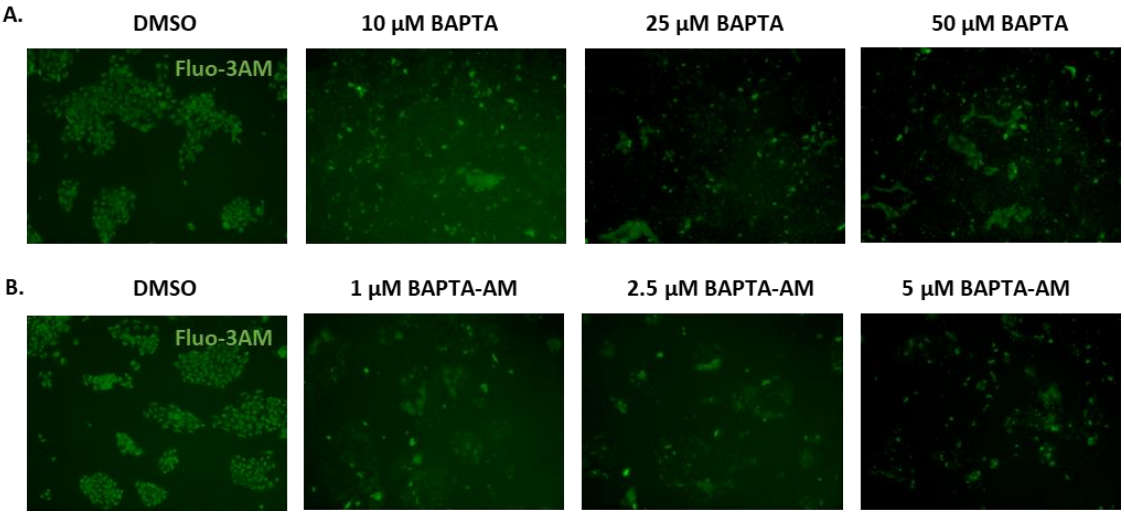

Figure 3.2.1 The Fluo-3AM signals of HaCaT cells expressing Cx26-G45E-GFP construct. (A) Fluo-3AM Ca^{2+} signals of G45E cells treated with corresponding volume of DMSO, 10 µM, 25 µM and 50 µM BAPTA. (B) Fluo-3AM Ca^{2+} signals of G45E cells treated with corresponding volume of DMSO, 1 µM, 2.5 µM and 5 µM BAPTA-AM (scale bar= 100µm).

3.2.2 Chelation of intracellular Ca^{2+} decreased the expression of NF-κB in HaCaT cells with Cx26 overexpression and Cx26 KID Syndrome mutations.

To understand the impact of reduction of intracellular Ca^{2+} in HaCaT cells expressing WT, G45E and D50Y constructs, on NF-κB signal activity, NF-κB -Luciferase reporter assay was conducted. Cells were treated with 5 µM BAPTA-AM and corresponding volume of DMSO for 6 hours. The fold differences were assessed by normalization to results of control MSCV cells treated with DMSO.

The NF-κB pathway activity was reduced by 50% in BAPTA-AM treated WT while there was slight decrease compared to control DMSO treated WT. Similarly, the NF-κB pathway activity revealed a slight decrease in BAPTA-AM treated G45E compared to DMSO treated G45E. The activity decreased by 88% in both DMSO and BAPTA-AM treated G45E. BAPTA-AM treated D50Y cells had 79% less NF-κB activity and less activity compared to control DMSO treated D50Y. Compared to BAPTA-AM treated WT cells, NF-κB activation dropped by 39% in BAPTA-AM treated G45E and 29% in BAPTA-AM treated D50Y cells (Figure 3.2.2; n=2). Overall, the NF-κB activation was low in BAPTA-AM treated cells.

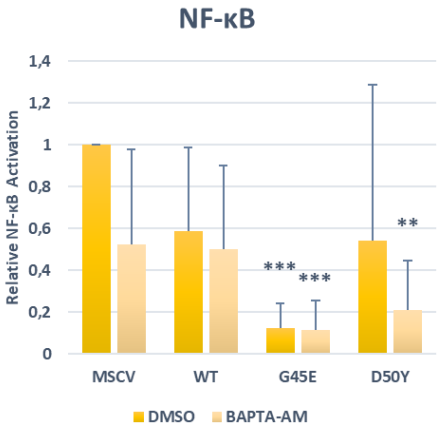

Figure 3.2.2. Relative NF-κB expression levels for MSCV, WT, G45E and D50Y after DMSO and 5 µM BAPTA-AM treatment with respect to DMSO-MSCV control cells (n=2, ± $p<0.1$; ** $p<0.01$; *** $p<0.005$). Statistical significance was assessed by unpaired t test (** $p<0.01$; *** $p<0.005$). The error bars represent the standard deviation.

3.2.3 Reduction of intracellular Ca^{2+} changed the expression pattern and activation of canonical NF-κB TFs in HaCaT cells overexpressing Cx26 WT and KID Syndrome mutations.

In order to understand how reduction of intracellular Ca^{2+} affects the expression and activation of NF-κB TFs in HaCaT cells expressing WT, G45E and D50Y, Western Blotting and q-RT-PCR experiments were conducted by treating cells with 5 μM BAPTA-AM and corresponding volumes of DMSO. The fold differences were assessed by normalization to control MSCV cells treated with DMSO. The expression of p65 was represented in Figure 3.2.3. p65 protein levels increased by 98% in BAPTA-AM treated MSCV. BAPTA-AM treated WT revealed the same levels of p65 expression with DMSO treated WT cells. p65 protein levels dropped by %68 in BAPTA-AM treated G45E compared to DMSO treated G45E. Also, it had less p65 protein levels compared to BAPTA-AM treated WT. BAPTA-AM treated and DMSO treated D50Y cells had same levels of p65 protein while 50% less p65 protein compared to WT(Figure 3.2.3.A; n=3). Depending on the q-RT-PCR results, DMSO treated D50Y cells indicated 38% decrease in p65 expression. WT and G45E cells did not indicate any significant change (Figure 3.2.3.A; n=3). In BAPTA-AM trials, p65 mRNA expression dropped by 30% in MSCV, 30% in G45E and 3% in D50Y compared to their control DMSO treated trials (Figure 3.2.3.B; n=4). WT did not indicate any significant change in p65 expression (Figure 3.2.3.3; n=4). The lowest expression of p65 protein and mRNA was indicated in both DMSO and BAPTA-AM treated D50Y cells.

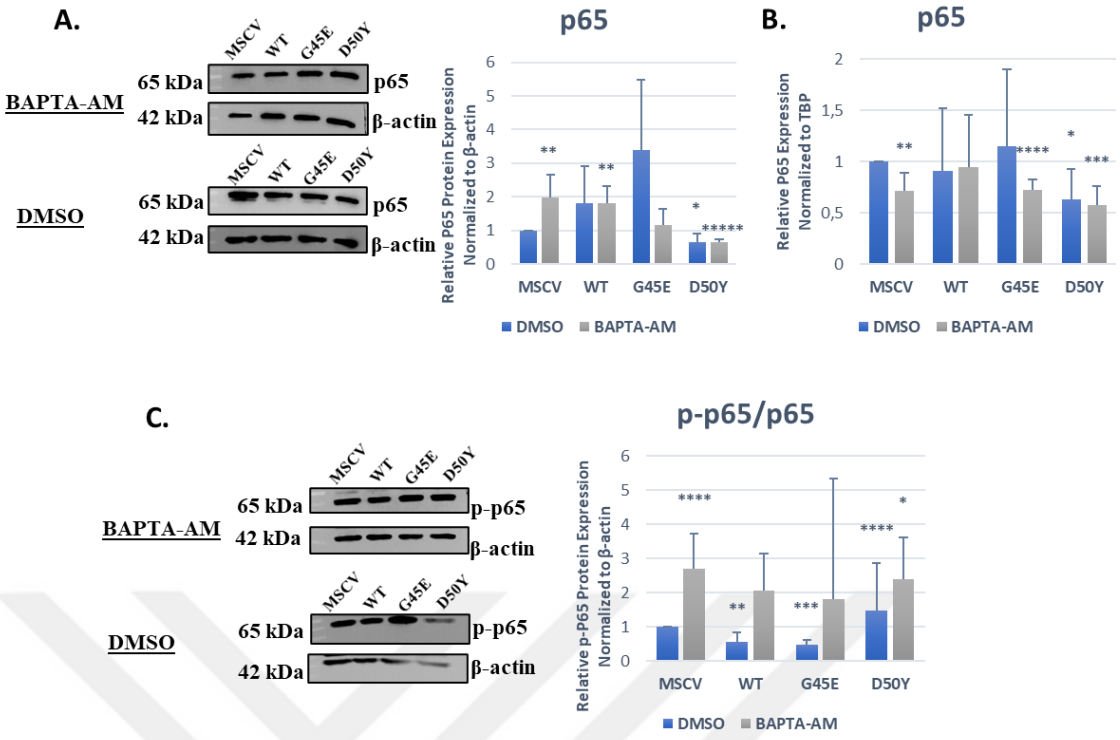

Figure3.2.3. p65 expression levels after 6 hours DMSO and 5 µM BAPTA-AM treatment for MSCV, WT, G45E and D50Y. (A) Relative p65 protein expression level for WT, G45E and D50Y cells with respect to control MSCV cells after DMSO and 5 µM BAPTA-AM treatment (n=3 , * p< 0.05; ** p< 0.01; ***** p< 0.0001) (B) Relative p65 mRNA expression level for WT, G45E and D50Y cells with respect to control MSCV cells after DMSO and 5 µM BAPTA-AM treatment (n=4 , * p<0.05; ** p<0.01; *** p<0.005; **** p< 0.001) (C) Relative p65 activation levels (p-p65 compared to p65 protein expression levels) for WT, G45E and D50Y cells with respect to control MSCV cells after DMSO and 5 µM BAPTA-AM treatment (n=3, * p<0.05; ** p<0.01; *** p<0.005; **** p< 0.001). Statistical significance was assessed by unpaired t test (* p<0.05; ** p<0.01; *** p<0.005; **** p< 0.001; ***** p< 0.0001). The error bars represent the standard deviation.

The activation of p65 protein was analyzed by p-p65 protein levels normalized to p65 protein levels of each group of cells. In DMSO trials, p-p65 expression reduced by half in WT and 53% in G45E while increased by 52% in D50Y. Compared to WT, G45E had no noticeable change while D50Y revealed an approximate 2-fold increase in p-p65 expression. In BAPTA-AM trials, p-p65 protein levels increased by approximately 2.5-fold in MSCV and approximately 40% in D50Y compared to their DMSO treated trials. BAPTA-AM treated WT and G45E groups had approximately 4-fold more p-p65 protein levels compared to their DMSO trials (Figure 3.2.3.C; n=3).

Another NF-κB pathway member, c-Rel was analyzed in the same manner. DMSO treated cells did not show any significant change in c-Rel protein expression BAPTA-AM treated MSCV showed decrease by 35% (Figure 3.2.4.A; n=2). In DMSO trials, c-Rel mRNA expression decreased by 30% in D50Y. In BAPTA-AM trials, c-Rel mRNA expression dropped by 57% in MSCV, 25% in WT, 88% in G45E and 40% in D50Y compared to their DMSO trials (Figure 3.2.4.B; n=4). Compared to WT, c-Rel mRNA expression was slightly lower in G45E and D50Y.

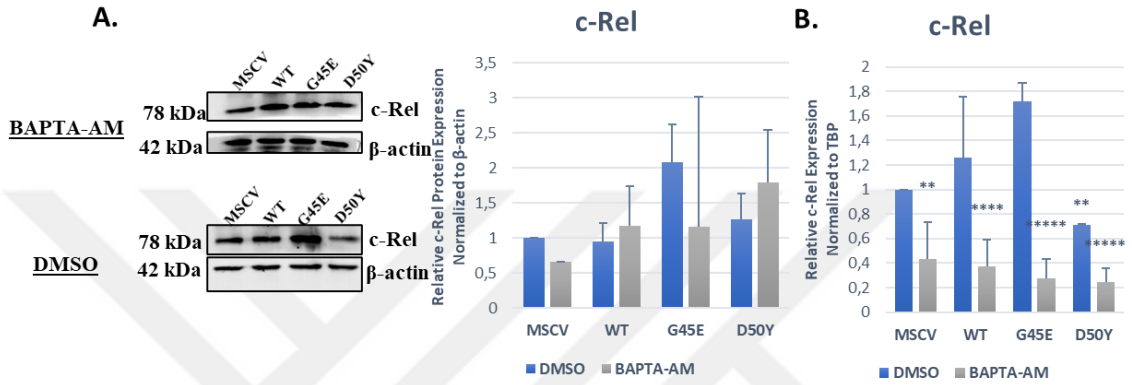

Figure 3.2.4.. c-Rel expression levels after 6 hours DMSO and 5 μM BAPTA-AM treatment for MSCV, WT, G45E and D50Y. (A) Relative c-Rel protein expression level for WT, G45E and D50Y cells with respect to control MSCV cells after DMSO and 5 μM BAPTA-AM treatment (n=2, ns) (B) Relative c-Rel mRNA expression level for WT, G45E and D50Y cells with respect to control MSCV cells after DMSO and 5 μM BAPTA-AM treatment (n=4, ** p <0.01; **** p<0.001; ***** p< 0.0001). Statistical significance was assessed by unpaired t test (** p<0.01; **** p< 0.001; ***** p< 0.0001). The error bars represent the standard deviation.

The main regulator of NF-κB pathway, IKK-γ was also analyzed in the same manner. Western Blotting results showed that DMSO treated G45E had 80% more expression compared to control DMSO treated MSCV cells. DMSO treated WT and D50Y (Figure 3.2.5.A; n=2) and BAPTA-AM treated MSCV, WT, G45E and D50Y cells did not indicate any significant change in IKK-γ protein levels (Figure 3.2.5.A; n=1). In q-RT-PCR results, BAPTA-AM treated MSCV cells had 53% low expression of IKK-γ mRNA (Figure 3.2.5.B; n=5). DMSO and BAPTA-AM treated WT, G45E and D50Y cells did not indicate any significant change in IKK-γ mRNA levels (Figure 3.2.5.B; n=5).

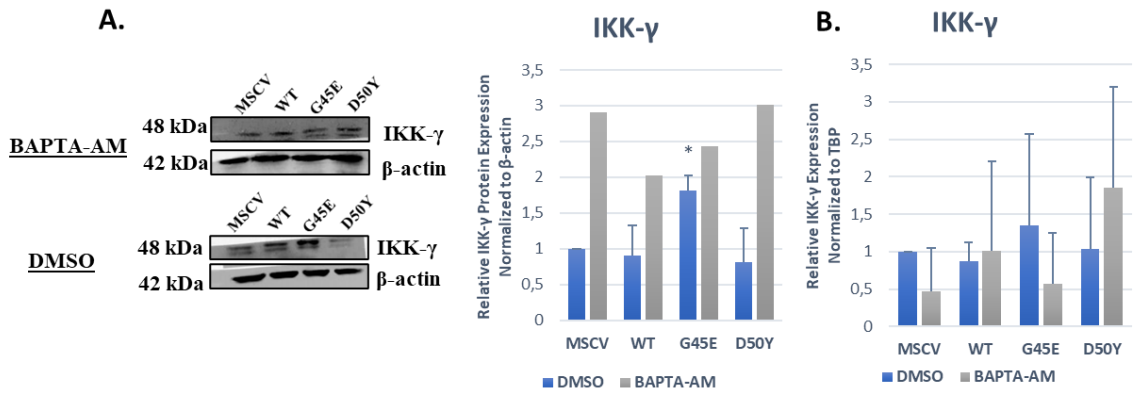

Figure 3.2.5. IKK-γ expression levels for MSCV, WT, G45E and D50Y after DMSO and 5 μM BAPTA-AM treatment. (A) Relative IKK-γ protein expression level for WT, G45E and D50Y cells with respect to control MSCV cells DMSO and 5 μM BAPTA-AM treatment (n=2, * p< 0.05) (B) Relative IKK-γ mRNA expression level for WT, G45E and D50Y cells with respect to control MSCV cells DMSO and 5 μM BAPTA-AM treatment (n=4). Statistical significance was assessed by unpaired t test (* p<0.05). The error bars represent the standard deviation.

Overall, reduced intracellular Ca^{2+} causes lower expression of p65 in D50Y cells while more expression in WT compared to control. The opposite results were found in activated p65, p-p65. Reduced intracellular Ca^{2+} causes lower c-Rel mRNA expression in each cell, specifically in D50Y. There is no difference among groups in IKK-γ expression.

3.2.4. Reduction of intracellular Ca^{2+} changed the expression pattern of non-canonical NF-κB TF among HaCaT cells Cx26 overexpression and Cx26 KID Syndrome mutations.

In the light of Western Blotting results, non-canonical NF-κB subunit, RelB decreased by approximately 50% in both DMSO and BAPTA-AM treated WT. DMSO and BAPTA-AM treated G45E and D50Y cells did not show any significant change in RelB protein expression (Figure 3.2.6.A; n=3). According to q-RT-PCR results, RelB mRNA expression increased by 68% in BAPTA-AM treated D50Y compared to DMSO treated D50Y; decreased 20% in BAPTA-AM treated G45E cells compared to DMSO treated G45E (Figure 3.2.6.B; n= 4). Meanwhile, DMSO treated WT and G45E cells, and BAPTA-AM treated MSCV, WT and D50Y cells did not indicate any significant change in RelB mRNA expression (Figure 3.2.6.B; n= 4).

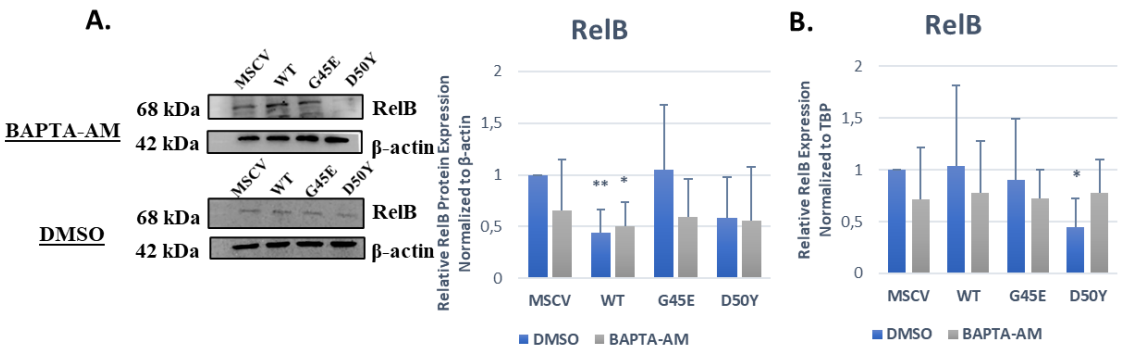

Figure 3.2.6. RelB expression levels for MSCV, WT, G45E and D50Y after DMSO and 5 μM BAPTA-AM treatment. (A) Relative RelB protein expression level for WT, G45E and D50Y cells with respect to control MSCV cells DMSO and 5 μM BAPTA-AM treatment (n=3, * $p< 0.05$; ** $p< 0.01$) (B) Relative RelB mRNA expression level for WT, G45E and D50Y cells with respect to control MSCV cells DMSO and 5 μM BAPTA-AM treatment (n=4, ± $p<0.1$; * $p<0.05$). Statistical significance was assessed by unpaired t test (* $p<0.05$; ** $p<0.01$). The error bars represent the standard deviation.

3.2.5. Reduction of intracellular Ca^{2+} changed the localization of NF-κB TFs among HaCaT cells with Cx26 overexpression and Cx26 KID Syndrome mutations.

The NF-κB pathway members activity can be also determined by examining their localization. The changes in nuclear translocation of p65, RelB and c-Rel varied among HaCaT cells expressing MSCV, WT, G45E and D50Y constructs with and without intracellular Ca^{2+}. The nuclear signals of p65 were reduced by 10% in DMSO treated G45E cells while DMSO treated WT and D50Y did not show any significant change. In BAPTA-AM trials, p65 nuclear signals increased by 15% in WT and decreased by approximately 30% in D50Y compared to their DMSO trials while there was no significant change in MSCV and G45e (Figure 3.2.7; n=2).

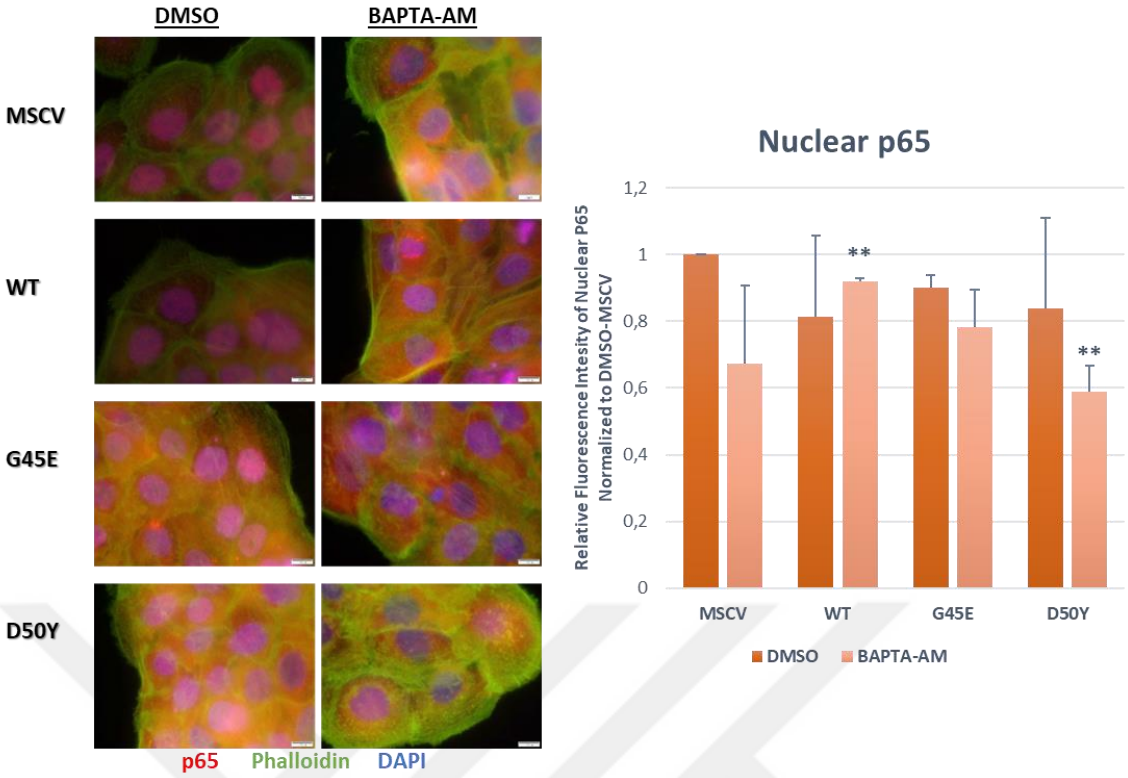

Figure 3.2.7 Localization of p65 in DMSO and 5 µM BAPTA-AM treated MSCV, WT, G45E and D50Y cells. The graph represents relative fluorescence intensity of nuclear p65 protein in DMSO and 5 µM BAPTA-AM treated MSCV, WT, G45E and D50Y cells in respect to DMSO-MSCV. Images were taken at 100X magnification (scale bar=10 µm, n=2, (± $p<0.1$; ** $p<0.01$) Statistical significance was assessed by unpaired t test (** $p<0.01$). The error bars represent the standard deviation.

The localization of another canonical NF-κB subunit, c-Rel was observed and found that BAPTA-AM treated MSCV had 20% more; D50Y had 10% less c-Rel nuclear signals compared to their respective DMSO controls. DMSO treated WT, G45E and D50Y cells and BAPTA-AM treated WT and G45E cells did not indicate any significant change (Figure 3.2.8; n=2).

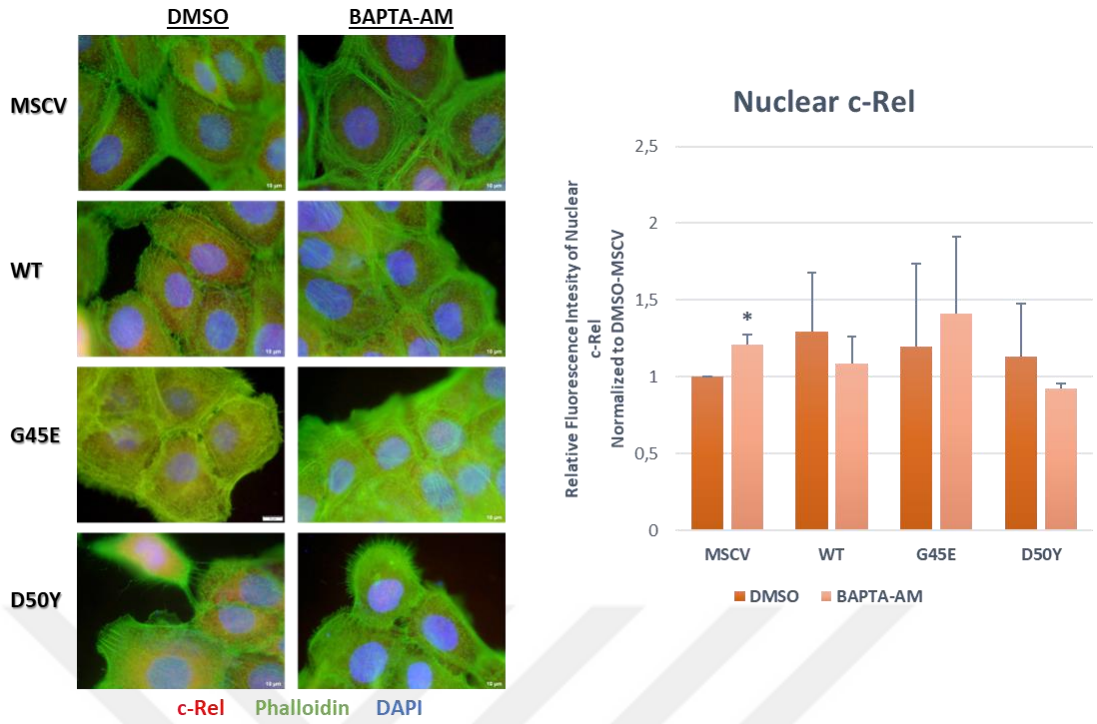

Figure3.2.8. Localization of c-Rel in DMSO and 5 µM BAPTA-AM treated MSCV, WT, G45E and D50Y cells. The graph represents relative fluorescence intensity of nuclear c-Rel protein in DMSO and 5 µM BAPTA-AM treated MSCV, WT, G45E and D50Y cells in respect to DMSO-MSCV. Images were taken at 100X magnification (scale bar=10 µm, n=2, * $p< 0.05$) Statistical significance was assessed by unpaired t test (* $p<0.05$). The error bars represent the standard deviation.

The nuclear signals of RelB were increased by approximately 2-fold in BAPTA-AM treated G45E and decreased by 12% in BAPTA-AM treated D50Y compared to their respective DMSO trials. Meanwhile, DMSO treated WT, G45E and BAPTA-AM treated MSCV, WT and G45E did not indicate any significant changes (Figure 3.2.9; n=2).

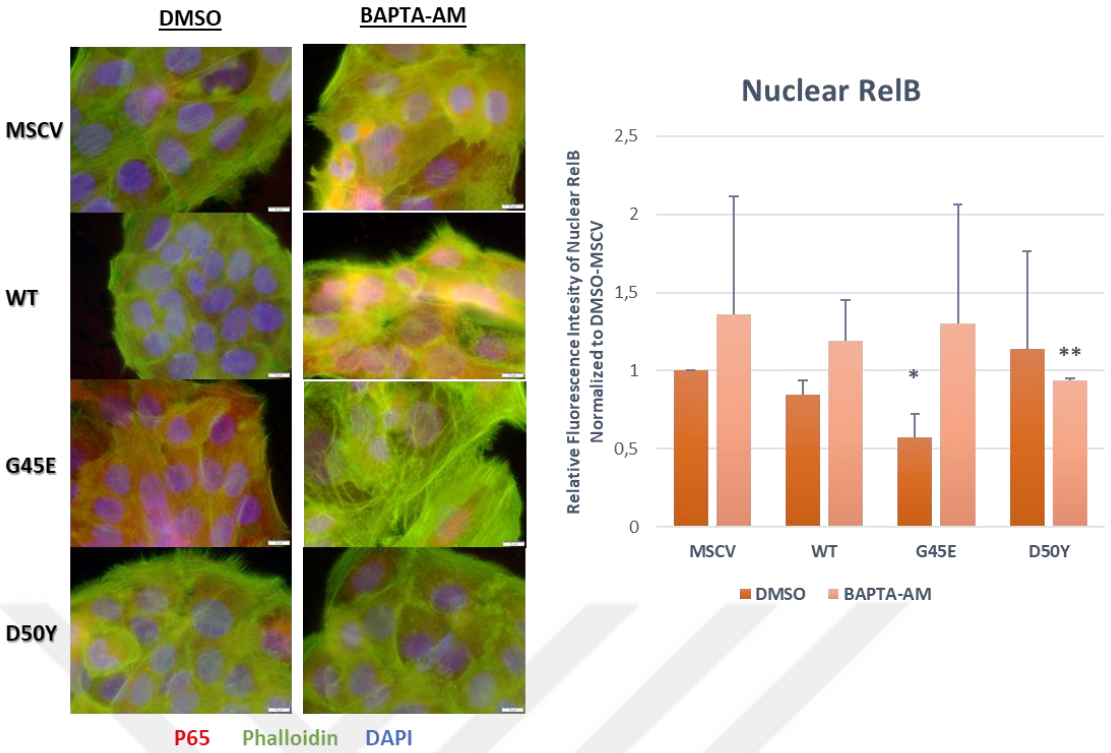

Figure3.2.9. Localization of RelB in DMSO and 5 µM BAPTA-AM treated MSCV, WT, G45E and D50Y cells. The graph represents relative fluorescence intensity of nuclear RelB protein in DMSO and 5 µM BAPTA-AM treated MSCV, WT, G45E and D50Y cells in respect to DMSO-MSCV. Images were taken at 100X magnification (scale bar=10 µm, n=2, * $p< 0.05$; ** $p<0.01$) Statistical significance was assessed by unpaired t test (* $p<0.05$; ** $p<0.01$). The error bars represent the standard deviation.

3.3. SECTION III

3.3.1. Reduction of extracellular Ca^{2+} changed the expression pattern of NF-κB among HaCaT cells with Cx26 overexpression and Cx26 KID Syndrome mutations.

To understand the impact of reduction of extracellular Ca^{2+} in HaCaT cells expressing WT, G45E and D50Y constructs, on NF-κB expression, NF-κB -Luciferase reporter assay was conducted. Cells were treated with 25 μM BAPTA and corresponding volume of DMSO for 6 hours. The fold differences were assessed by normalization to NF-κB expression results of control MSCV cells treated with DMSO.

The NF-κB expression was increased by 18% in BAPTA treated G45E compared to DMSO treated G45E (Figure 3.2.9; n=2). DMSO and BAPTA treated MSCV, WT, and D50Y cells did not indicate any significant changes. In addition, the NF-κB expression pattern was similar among groups with previous experiments; the lowest in G45E and high in D50Y.

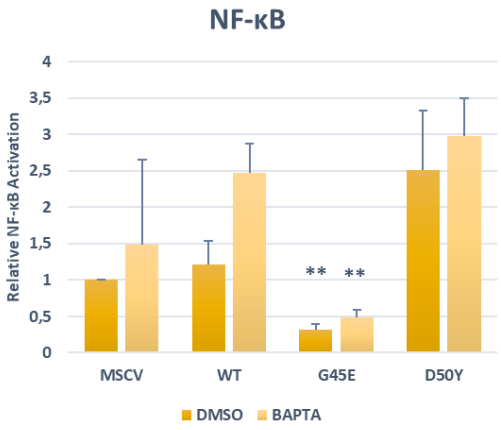

Figure 3.3.1. Relative NF-κB expression levels for MSCV, WT, G45E and D50Y after DMSO and 25 μM BAPTA treatment with respect to DMSO-MSCV control cells (n=2, ** $p<0.01$). Statistical significance was assessed by unpaired t test (** $p<0.01$). The error bars represent the standard deviation.

3.3.2. Reduction of extracellular Ca^{2+} changed the expression pattern, activation, and localization of canonical NF-κB TFs among HaCaT cells with Cx26 overexpression and Cx26 KID Syndrome mutations.

To understand how reduction of extracellular Ca^{2+} affects the expression and activation of NF-κB TFs in HaCaT cells expressing WT, G45E and D50Y, Western Blotting and q-RT-PCR experiments were conducted by treating cells with 25 μM BAPTA and corresponding volumes of DMSO. The fold differences were assessed by normalization to control MSCV cells treated with DMSO. In BAPTA treated trials, p65 protein levels decreased by approximately half in MSCV; 70% in WT and 40% in G45E compared to their respective control DMSO trials (Figure 3.3.2.A; n=3). Compared to BAPTA treated WT, p65 protein expression increased by approximately 70% in G45E. Based on the q-RT-PCR results, in BAPTA trials, p65 mRNA expression dropped by 14% in MSCV, 42% in WT and 36% in D50Y compared to their respective control DMSO trials (Figure 3.3.2.B; n=3). G45E did not indicate any significant change in p65 expression. The lowest expression of p65 protein and mRNA was indicated in BAPTA treated WT and D50Y cells.

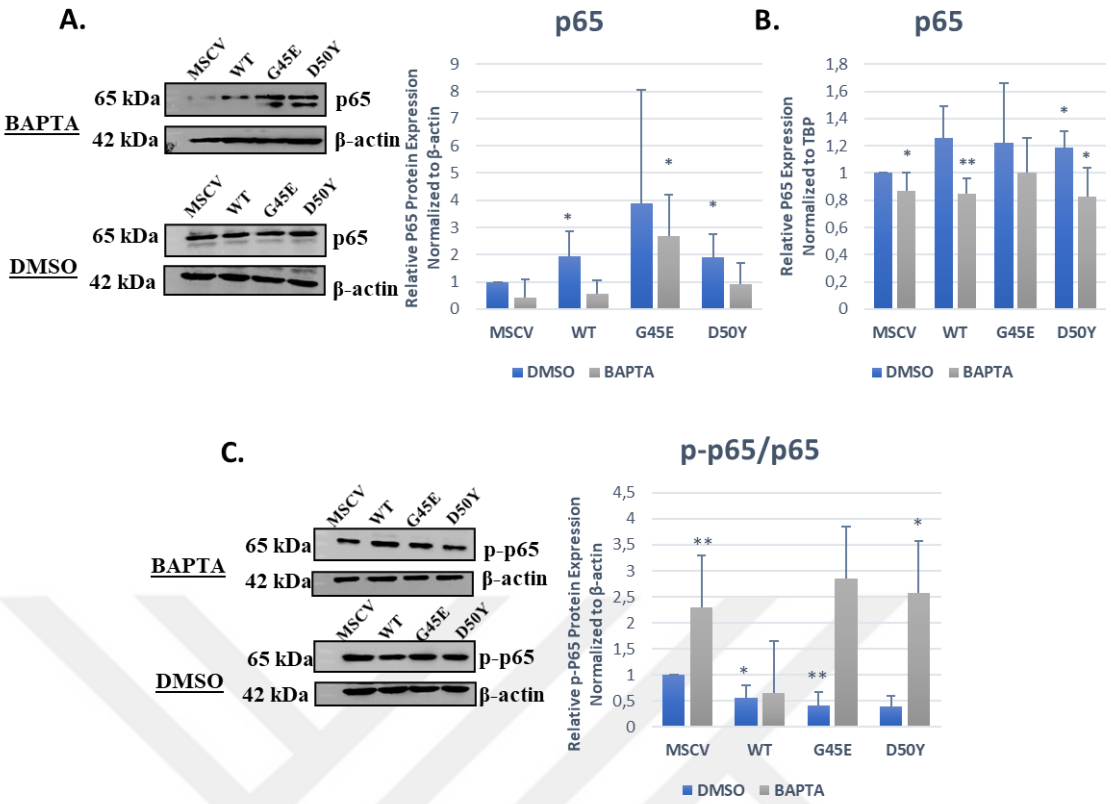

Figure 3.3.2. p65 expression levels after 6 hours DMSO and 25 µM BAPTA treatment for MSCV, WT, G45E and D50Y. (A) Relative p65 protein expression level for WT, G45E and D50Y cells with respect to control MSCV cells after DMSO and 25 µM BAPTA treatment (n=3, * p< 0.05) (B) Relative p65 mRNA expression level for WT, G45E and D50Y cells with respect to control MSCV cells after DMSO and 25 µM BAPTA treatment (n=3, * p <0.05; ** p<0.01) (C) Relative p65 activation levels (p-p65 compared to p65 protein expression levels) for WT, G45E and D50Y cells with respect to control MSCV cells after DMSO and 25 µM BAPTA treatment (n=3, * p <0.05; ** p<0.01). Statistical significance was assessed by unpaired t test (* p<0.05; ** p<0.01). The error bars represent the standard deviation.

The activation of p65 protein was analyzed by p-p65 protein levels normalized to p65 protein levels of each group of cells. In DMSO trials, p-p65 expression reduced by 44% in WT and 59% in G45E (Figure 3.3.2.C; n=3). Compared to WT, G45E had lower p-p65 expression. In BAPTA trials, p-p65 protein levels increased by approximately 2.5-fold in both MSCV; 8-fold in G45E and 7-fold in D50Y compared to their respective DMSO trials (Figure 3.3.2.C; n=3). WT had lower p-p65 expression compared to G45E and D50Y. There was no significant change between control DMSO and BAPTA treated in WT.

Another NF-κB subunit, c-Rel was analyzed in the same manner. DMSO and BAPTA treated WT, G45E and D50Y cells did not show any significant change in c-Rel

protein expression. BAPTA treated MSCV showed 59% decrease (Figure 3.3.3.A; n=3). Based on q-RT-PCR results, in BAPTA trials, c-Rel mRNA expression dropped by 34% in MSCV, approximately 50% in WT and D50Y compared to their respective DMSO trials (Figure 3.3.3.B; n=3). Compared to WT, c-Rel mRNA expression was slightly higher in D50Y.

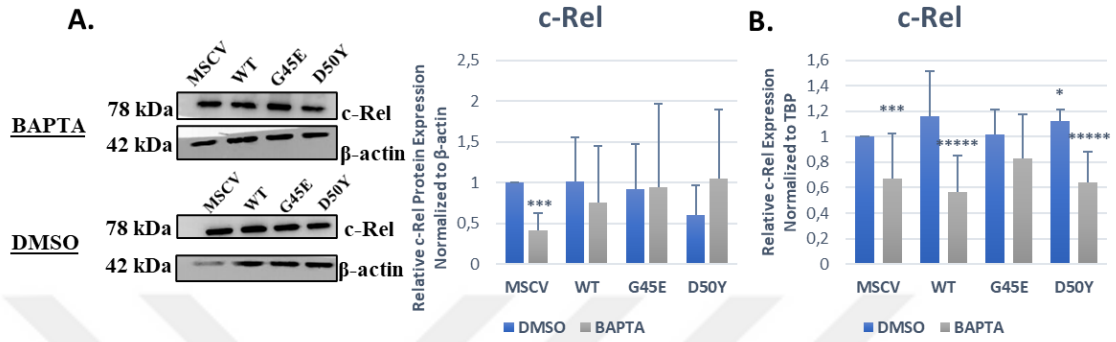

Figure 3.3.3. c-Rel expression levels after 6 hours DMSO and 25 μM BAPTA treatment for MSCV, WT, G45E and D50Y. (A) Relative c-Rel protein expression level for WT, G45E and D50Y cells with respect to control MSCV cells after DMSO and 25 μM BAPTA treatment (n=3, *** $p< 0.005$) (B) Relative c-Rel mRNA expression level for WT, G45E and D50Y cells with respect to control MSCV cells after DMSO and 25 μM BAPTA treatment (n=3, * $p <0.05$; *** $p<0.005$; ***** $p< 0.0001$). Statistical significance was assessed by unpaired t test (* $p<0.05$; *** $p<0.005$; ***** $p< 0.0001$). The error bars represent the standard deviation.

The main regulator of NF-κB pathway, IKK-γ was analyzed in the same manner. Western Blotting results showed that DMSO treated D50Y had approximately 4-fold increase (Figure 3.3.4.A; n=2). BAPTA treated MSCV cells had almost zero expression of IKK-γ compared to DMSO treated MSCV cells. BAPTA treated D50Y had slightly more protein levels compared to DMSO trial (Figure 3.3.4.A; n=2). DMSO and BAPTA treated D50Y had more protein levels compared to WT. In q-RT-PCR results, IKK-γ mRNA expression dropped by 33% in DMSO treated WT and 28% in DMSO treated D50Y (Figure3.3.4.B; n=3). BAPTA treated MSCV cells had 31% less expression of IKK-γ mRNA while D50Y had similar expression compared to their respective DMSO trials (Figure3.3.4.B; n=3). Compared to WT, expression levels were similar in DMSO and BAPTA treated D50Y.

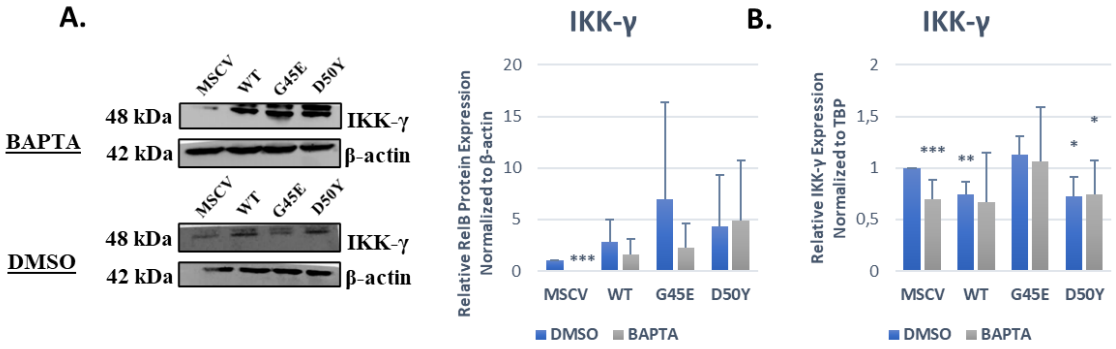

Figure 3.3.4. IKK-γ expression levels for MSCV, WT, G45E and D50Y after DMSO and 25 μM BAPTA treatment. (A) Relative IKK-γ protein expression level for WT, G45E and D50Y cells with respect to control MSCV cells DMSO and 25 μM BAPTA treatment (n=2, *** p< 0.005) (B) Relative IKK-γ mRNA expression level for WT, G45E and D50Y cells with respect to control MSCV cells DMSO and 25 μM BAPTA treatment (n=3, * p<0.05; ** p<0.01; *** p<0.005;). Statistical significance was assessed by unpaired t test (* p<0.05; ** p<0.01; *** p<0.005). The error bars represent the standard deviation.

Overall, reduction of extracellular Ca^{2+} causes lower expression of p65 in WT cells while more expression in G45E compared to control. The activation of p65 was higher in D50Y in reduced extracellular Ca^{2+}. Reduction of extracellular Ca^{2+} causes lower c-Rel mRNA expression specifically in D50Y. IKK-γ expression obtained similar in DMSO and BAPTA treated D50Y.

3.3.3. Reduction of extracellular Ca^{2+} changed the expression pattern of non-canonical NF-κB TFs among HaCaT cells with Cx26 overexpression and Cx26 KID Syndrome mutations.

Due to Western Blotting results, non-canonical NF-κB subunit, RelB decreased by 52% in BAPTA treated WT compared to DMSO treated WT (Figure 3.3.5.A; n=3). RelB protein levels reduced by 72% in BAPTA treated MSCV and approximately 40% in BAPTA treated D50Y compared to their respective DMSO trials (Figure 3.3.5.A; n=3). DMSO treated G45E and D50Y, and BAPTA treated G45E cells did not show any significant change in RelB protein expression (Figure 3.3.5.A; n=3). DMSO and BAPTA treated D50Y had similar protein levels compared to DMSO and BAPTA treated WT. According to q-RT-PCR results, RelB mRNA expression dropped by 30% in BAPTA treated WT, 9% in BAPTA treated G45E and 30% in BAPTA treated D50Y compared to

their respective DMSO trials (Figure 3.3.5.B; n=3). G45E had higher, D50Y had lower RelB mRNA expression compared to WT in both DMSO and BAPTA trials.

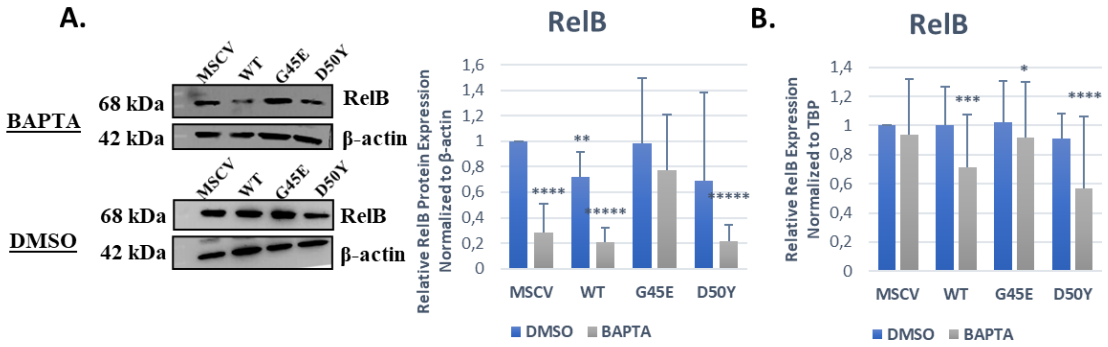

Figure 3.3.5. RelB expression levels for MSCV, WT, G45E and D50Y after DMSO and 25 µM BAPTA treatment. (A) Relative IKK-γ protein expression level for WT, G45E and D50Y cells with respect to control MSCV cells DMSO and 25 µM BAPTA treatment (n=3, ** p< 0.01; **** p< 0.001; ***** p< 0.0001) (B) Relative IKK-γ mRNA expression level for WT, G45E and D50Y cells with respect to control MSCV cells DMSO and 25 µM BAPTA treatment (n=3, * p<0.05; *** p<0.005; **** p<0.001;). Statistical significance was assessed by unpaired t test (* p<0.05; ** p<0.01; *** p<0.005; **** p< 0.001; ***** p< 0.0001). The error bars represent the standard deviation.

3.3.4. Reduction of extracellular Ca^{2+} changed the expression localization of NF-κB TFs among HaCaT cells with Cx26 overexpression and Cx26 KID Syndrome mutations.

The changes in nuclear translocation of p65, RelB and c-Rel varied among HaCaT cells expressing MSCV, WT, G45E and D50Y constructs with and without extracellular Ca^{2+}. The nuclear signals of p65 increased by 47% in BAPTA treated MSCV and 35% in BAPTA treated D50Y cells compared to their respective DMSO trials (Figure 3.3.6; n=2). Compared to WT, D50Y had more p65 nuclear signal.

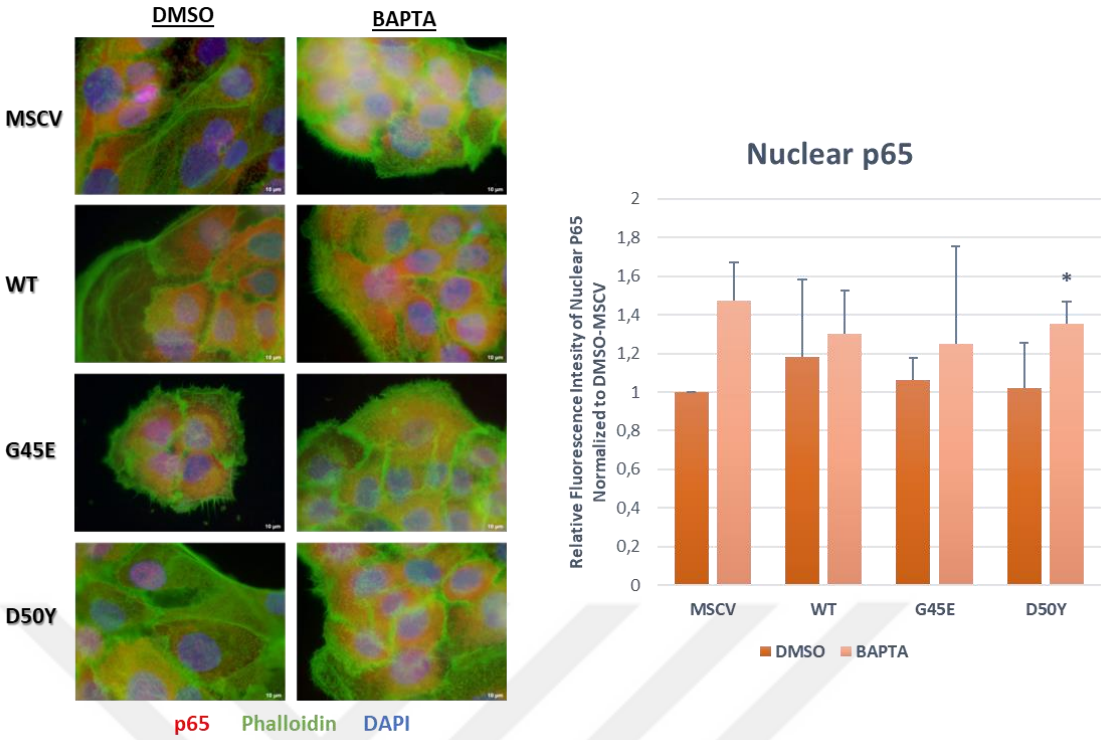

Figure 3.3.6. Localization of p65 in DMSO and 25 µM BAPTA treated MSCV, WT, G45E and D50Y cells. The graph represents relative fluorescence intensity of nuclear p65 protein in DMSO and 25 µM BAPTA treated MSCV, WT, G45E and D50Y cells in respect to DMSO-MSCV. Images were taken at 100X magnification (scale bar=10 µm, n=2, * $p< 0.05$) Statistical significance was assessed by unpaired t test (* $p<0.05$). The error bars represent the standard deviation.

The localization of another canonical NF-κB TF, c-Rel was observed and found that BAPTA treated G45E exhibited a 5% reduction, and BAPTA treated D50Y showed an 8% decrease in c-Rel nuclear signals compared to their respective DMSO trials (Figure 3.3.7; n=2). Compared to BAPTA treated WT, BAPTA treated G45E had slightly more, D50Y had less c-Rel nuclear signals.

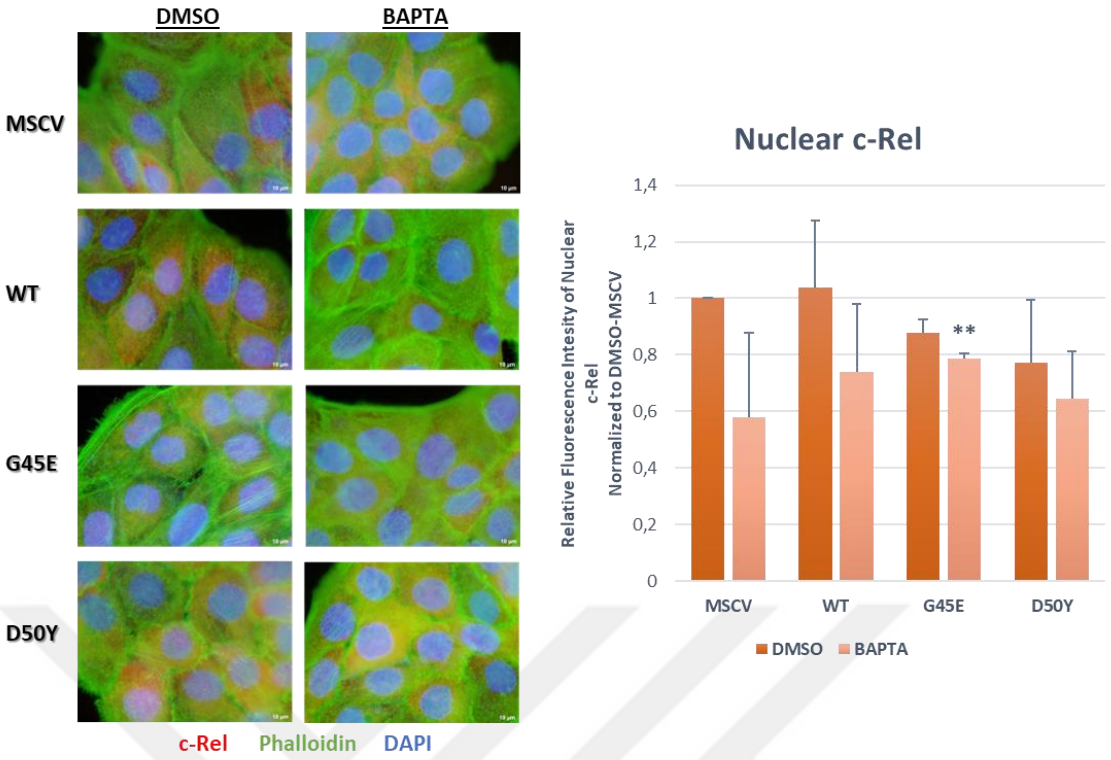

Figure 3.3.7. Localization of RelB in DMSO and 25 μM BAPTA treated MSCV, WT, G45E and D50Y cells. The graph represents relative fluorescence intensity of nuclear RelB protein in DMSO and 25 μM BAPTA treated MSCV, WT, G45E and D50Y cells in respect to DMSO-MSCV. Images were taken at 100X magnification (scale bar=10 μm, n=2, ** p< 0.01) Statistical significance was assessed by unpaired t test (** p<0.01). The error bars represent the standard deviation.

The nuclear signals of RelB were increased by 70% in BAPTA treated MSCV (Figure 3.3.8; n=2). BAPTA treated WT exhibited an approximate 10% reduction in RelB nuclear signal compared to DMSO treated WT. Meanwhile, DMSO treated G45E and D50Y, and BAPTA treated WT, G45E, and D50Y did not indicate any significant change (Figure 3.3.8; n=2). Compared to BAPTA treated WT, BAPTA treated G45E and D50Y had more RelB nuclear signals.

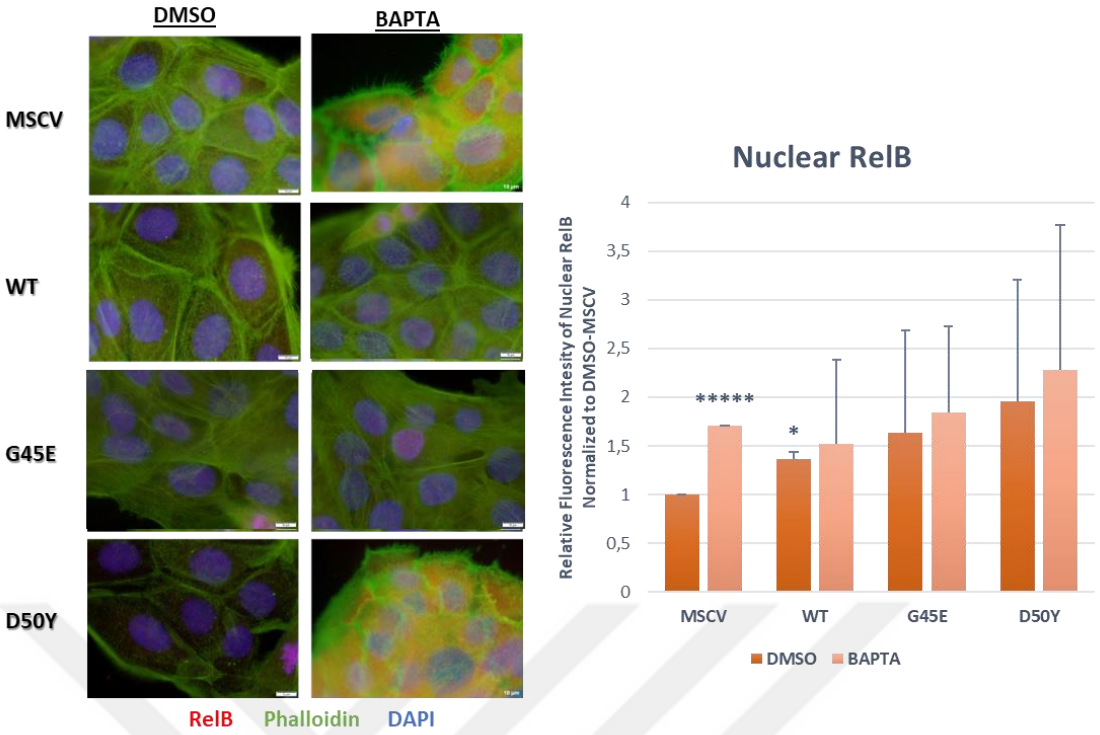

Figure 3.3.8. Localization of RelB in DMSO and 25 µM BAPTA treated MSCV, WT, G45E and D50Y cells. The graph represents relative fluorescence intensity of nuclear RelB protein in DMSO and 25 µM BAPTA treated MSCV, WT, G45E and D50Y cells in respect to DMSO-MSCV. Images were taken at 100X magnification (scale bar=10 µm, n=2, * $p< 0.05$; ***** $p< 0.0001$) Statistical significance was assessed by unpaired t test (* $p<0.05$; ***** $p< 0.0001$). The error bars represent the standard deviation.

CHAPTER 4

DISCUSSION AND CONCLUSION

In this study, we investigated effects of impaired Ca^{2+} homeostasis due to Cx26 overexpression and Cx26 KID syndrome mutations expressing keratinocytes on NF-κB pathway. Cx26 KID syndrome mutations revealed different phenotypes such as G45E caused lethality while D50Y caused hyperproliferation (Jonard et al., 2008; Aypek et al., 2016). Based on the literature, there are three topics related to keratinocytes homeostasis; i) among 12 Cx26 KID syndrome mutations, both G45E and D50Y characterized by aberrant hemichannel activity by extracellular Ca^{2+} but revealed opposite phenotypes (Jonard et al., 2008; Aypek et al., 2016; Lilly et al., 2019), ii) Ca^{2+} homeostasis is crucial for epidermal growth and mutated Cx26 channels proposed aberrant Ca^{2+} homeostasis (Tu et al., 2012; Srinivas et al., 2018), iii) similar to Ca^{2+}, NF-κB pathway also mediates keratinocyte physiology (Takao, 2003; Wullaert et al., 2011; Shen et al., 2023) and several studies showed that Ca^{2+} regulates NF-κB activation directly or indirectly (Berry et al., 2018). In our study, we discussed these three issues together in keratinocytes expressing Cx26 WT, G45E and D50Y KID syndrome mutations.

Table 4.1. Summary of the expression of NF-κB pathway members based on our results.

		Normal Conditions		Reduced intracellular Ca^{2+}			Reduced extracellular Ca^{2+}		
		Protein levels	mRNA expression	Protein levels	mRNA expression	Nuclear Signal	Protein levels	mRNA expression	Nuclear Signal
p65	WT	↓	↓	↑	↓	↓	↓	↓	
	G45E								
	D50Y		↓	↓	↓	↓		↓	↑
p-p65	WT	↑							
	G45E	↑							
	D50Y			↑			↑		
c-Rel	WT							↓	
	G45E	↑	↑		↓				↓
	D50Y		↓		↓	↓		↓	↓
IKK-γ	WT								
	G45E	↓							
	D50Y		↓					↓	
RelB	WT	↓	↓	↓			↓	↓	
	G45E		↓		↓			↓	
	D50Y	↓	↓			↓	↓	↓	

Cx26 expression profile and NF-κB activation were checked among cells and Cx26 overexpression, WT and D50Y groups had increased Cx26 expression and NF-κB activation. As mentioned before, G45E mutation causes lethality (Mese et al., 2011). The reason for less Cx26 expression might be that cells did not prefer to express lethal G45E mutation carrying Cx26 gene. G45E had the lowest NF-κB activation among cells. In keratinocytes, NF-κB was related to keratinocyte proliferation while it inhibited apoptosis (Wullaert et al., 2011; Fullard et al., 2013; Grinberg-Bleyer et al., 2015). In this case, the presence of G45E lethal mutation and the activation of NF-κB pathway seemed negatively correlated as expected.

The NF-κB pathway is a multifunctional protein pathway that is also regulated by itself, and has been proved by several studies that it plays a role in proliferation and differentiation of keratinocytes (Z. J. Li et al., 2013; Grinberg-Bleyer et al., 2015; Zhang et al., 2017) .Therefore, the expression of each member of canonical and non-canonical NF-κB pathways were investigated in Cx26 WT and KID syndrome mutation groups. WT and D50Y mutation groups had decreased p65 expression. In contrast, the activated p65, p-p65 was high in WT while G45E had lower p-p65. p65 deficiency was

characterized by impaired epidermal growth (Kim & Pasparakis, 2014). Compared to WT, it was expected to see lethal G45E had lower p65 activation. Like the other NF-κB member, p65, c-Rel expression was less in D50Y while the expression of both c-Rel and p-p65 was high in G45E. c-Rel maintains keratinocyte proliferation and inflammation (Fullard et al., 2013). However, our study demonstrated the opposite relationship between c-Rel expression Cx26 mutations phenotypes. As mentioned before, NF-κB pathway is multifunctional regulator of cell physiology. It has been shown that c-Rel can both induce and inhibit apoptosis in a cell by resisting TNF-α induced apoptosis and increasing apoptosis via manganese superoxide dismutase (MnSOD) (Bernard et al., 2002). Our study did not reveal how keratinocytes goes under apoptosis or not, but it was known that induced NF-κB activation causes MnSOD upregulation and cell death in keratinocytes (Deruy et al., 2010). This might explain the unexpected c-Rel upregulation in lethal KID syndrome mutation carrying cells but downregulation in hyperproliferative KID syndrome mutation carrying keratinocytes. IKK-γ is starter point of NF-κB pathway and found as downregulated in both G45E and D50Y groups. It has been shown that G45E and D50Y had lower p65 activation. Therefore, it was expected to observe less IKK-γ levels, as well. The reason is, it has been shown that NF-κB pathway had negative feedback regulatory system. IκB which is a NF-κB inhibitor is upregulated by activated p65 binding ((Di et al., 2012). In non-canonical pathway, RelB was investigated and found as downregulated in WT and even less in G45E and D50Y. This might be explained by the increased cell proliferation property of WT and D50Y. Especially for D50Y, such a protein linked to differentiation and inflammation (Havouis et al., 2000), it was expected to see as downregulated in hyperproliferation linked KID syndrome mutation expressing keratinocytes.

An important aspect of the NF-κB pathway is the intricate regulation among its members. For instance, it has been demonstrated that p50 (a dimer of p65 and c-Rel, which translocate to the nucleus together) collaborates with RelB in skin inflammation, even though they belong to different NF-κB pathways (Weih et al., 1997). Likewise, the non-canonical pathway regulator NIK has the capacity to activate both the IKK complex and directly phosphorylate p65 (Pflug & Sitcheran, 2020). Moreover, binding sites for p50, p65, and RelB have been identified in the NF-κB gene (Bren et al., 2001). It has also been revealed that c-Rel acts as its own regulator (Hannink, 1990). The reason of

decreased expression of NF-κB pathway members and activation of p65 in D50Y might be explained by this complex regulatory system.

In summary, in WT cells, there was an upregulation in proliferation-related canonical NF-κB transcription factors, specifically p65, and a downregulation in non-canonical NF-κB transcription factors, RelB. In hyperproliferation-linked D50Y cells, there was lower expression of all NF-κB members, but an upregulation in NF-κB activation. The upregulation of the NF-κB gene may be facilitated by other factos such as NIK and cAMP (Wittwer & Schmitz, 2008; Gerlo et al., 2011).

The relationship between Ca^{2+} and NF-κB in Cx26 KID syndrome expressing keratinocytes. To prevent Ca^{2+} from binding to its target proteins, Ca^{2+} chelators were employed. In trials with reduced intracellular Ca^{2+}, a decrease in NF-κB activation was observed in all groups, with activation levels varying from lower to higher in the order of G45E, D50Y, and WT. This reduction in NF-κB activation in a reduced intracellular Ca^{2+} environment aligns with the established positive correlation between Ca^{2+} and NF-κB, as supported by numerous studies conducted in keratinocytes and other cell types (Mogensen et al., 2003; Shinzawa et al., 2015; Yong et al., 2022). As illustrated in Figure 4.1, Ca^{2+} plays a role in the direct or indirect regulation of NF-κB pathway activation and the nuclear localization of NF-κB transcription factors in lymphocytes (Berry et al., 2018).

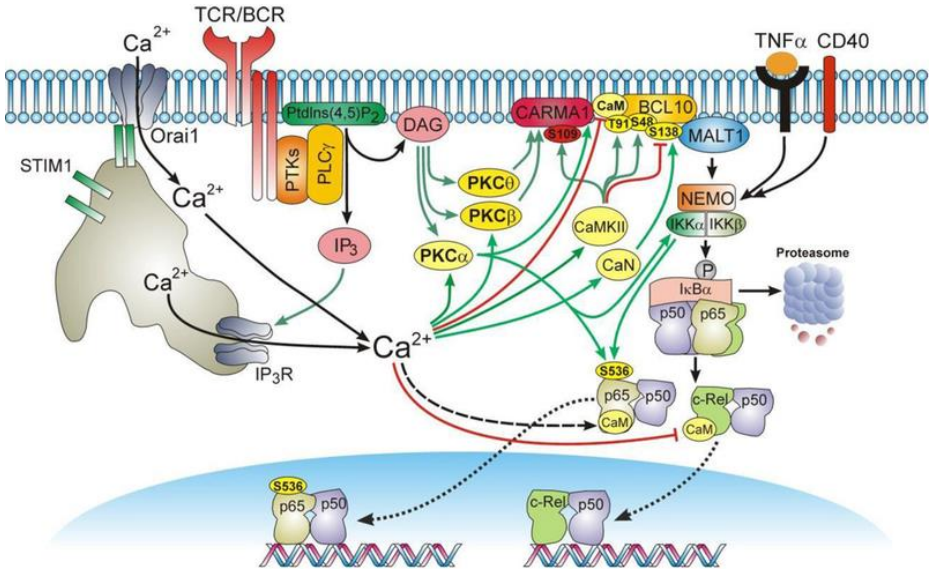

Figure 4.1. The direct or indirect effect of calcium on the NF-Kb protein pathway is demonstrated (Berry et al., 2018).

In keratinocytes, calmodulin (CaM) dependent kinases (CaMK) played a key role in regulating NF-κB pathway (Berry et al., 2018). CaMK4 was found as a positive regulator of NF-κB activation through AKT pathway in both keratinocytes and dermal macrophages to induce proliferation and avoid apoptosis (Yong et al., 2022). In addition, another Ca^{2+} ion transporter, transient receptor protein (TRPV3) induced intracellular Ca^{2+} increase and upregulated Ca^{2+}/CaMK2 which activated NF-κB through epidermal growth factor receptor (EGFR) and PI3K (Figure 4.2) (Wong et al., 2016). Hence, inhibiting the binding of intracellular Ca^{2+} could potentially diminish NF-κB activation in each group. In the case of keratinocytes expressing G45E, the substantial reduction in NF-κB activation may be attributed to the inhibitory effect of the deleterious G45E mutation on proliferation, as proliferation is positively associated with activated NF-κB pathway. G45E already exhibited low NF-κB activation under physiological conditions, and further reducing intracellular Ca^{2+} prevented NF-κB activation even more.

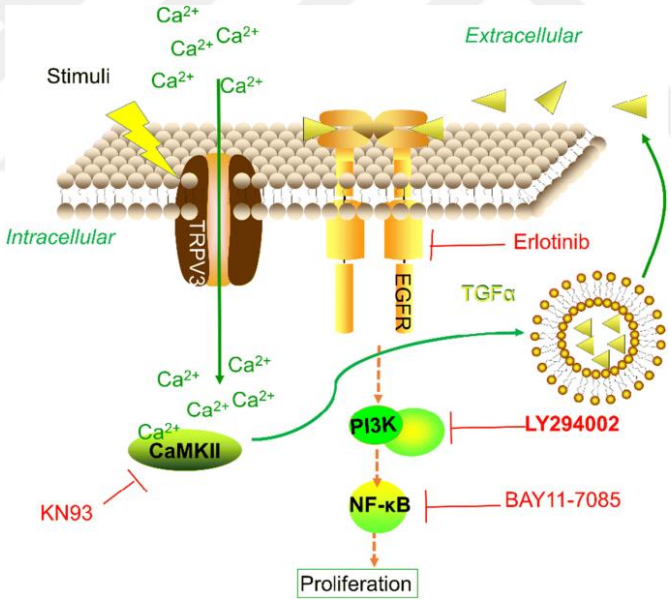

Figure 4.2. TRPV3 induced intracellular Ca^{2+} upregulated Ca^{2+}/CaMK2 which activated NF-κB through EGFR and PI3K (Wong et al., 2016).

G45E led to aberrant channel formation, cell lysis and increased Ca^{2+} permeability (Gerido et al., 2007; Sánchez et al., 2010). Similarly, D50Y led to destabilizing Cx26 hemichannel closure by extracellular Ca^{2+} and caused constantly open hemichannels (Lopez et al., 2013). It is expected to see increased intracellular Ca^{2+} levels in both mutations due to constantly open hemichannels since they transport Ca^{2+}. The difference

is, G45E had severe phenotypes that promotes cell death while D50Y was linked with hyperproliferation. It has been observed that G45E had lower NF-κB activation compared to D50Y. This showed that lethal G45E mutation revealed its phenotype through low NF-κB activation via aberrant Ca^{2+} homeostasis or aberrant transport of other Cx26 mediated molecules, such as cAMP, ATP etc (Gerlo et al., 2011; Chen et al., 2022).

The expression of NF-κB members was influenced by the reduction of intracellular Ca^{2+}. In WT and D50Y expressing keratinocytes, no significant changes were observed compared to their respective controls, except for D50Y, which showed lower p65 expression compared to WT. However, the activation levels of p65 and p-p65 increased in WT and D50Y compared to their respective controls. D50Y exhibited even higher p-p65 levels compared to WT. In contrast, G45E displayed lower p-p65 levels when intracellular Ca^{2+} was reduced. The results of NF-κB activation and p65 activation were in line with each other in the case of G45E. Given that p65 promotes proliferation (Kim & Pasparakis, 2014; Grinberg-Bleyer et al., 2015), it was expected to observe low NF-κB and p65 activation in the lethal G45E. However, WT and D50Y exhibited higher p65 activation in the reduced intracellular environment compared to their NF-κB activation results. This suggests that NF-κB activation might be regulated by $Ca^{2+}$and other molecules transported by Cx26, such as cAMP and ATP. Previous studies have shown that cAMP and ATP can suppress NF-κB pathway activation in lymphocytes (Hershfield, 2005). The gating of these molecules might suppress NF-κB activation in D50Y, although it does not explain the increased p65 phosphorylation in the reduced intracellular Ca^{2+}. This is because Ca^{2+} has been suggested as a positive regulator of p65 activation (Antonsson et al., 2003; Berry et al., 2018). Nuclear localization of p65 was high in WT but low in D50Y, contrasting with the high p65 activation in the reduced intracellular Ca^{2+}. Intracellular Ca^{2+} promotes the nuclear localization of p65 via CaM (Berry et al., 2018). This, coupled with increased p65 activation in D50Y, even as p-p65 levels increased, indicates that nuclear localization requires intracellular Ca^{2+}.

Extracellular Ca^{2+} was indicated as a regulator of Cx26 hemichannel gating. It has been shown that aberrant gating of G45E and D50Y mutation including Cx26 hemichannels were closed by binding of extracellular Ca^{2+} via changing the structure of pore lumen (Sánchez et al., 2010; Aypek et al., 2016; Lilly et al., 2019). In reduction of extracellular Ca^{2+}, G45E had more NF-κB activation (Fig 3.3.1). It might be explained by opening of mutated Cx26 hemichannels in reduced Ca^{2+} environment might cause

other molecules' transport, including free Ca^{2+}, cAMP and ATP. Also, depletion of extracellular Ca^{2+} storage may trigger the release of intracellular Ca^{2+} via Ca^{2+} stores, ER and mitochondria (Bikle & Mauro, 2014). Therefore, intracellular Ca^{2+} levels might be restored in reduced extracellular Ca^{2+} and promoted NF-κB activation. Even reduced intracellular Ca^{2+} did not affect p65 expression, reduction of extracellular Ca^{2+} caused lower expression of p65 in WT and D50Y and robust p65 activation in G45 and D50Y. As previously mentioned, opening of mutated Cx26 hemichannels might cause restoration of intracellular Ca^{2+} and promotes the activation of p65. This was also observed in increased nuclear localization of p65 in D50Y.

In contrast, c-Rel expression was significantly low in all keratinocytes in reduced intracellular Ca^{2+}. c-Rel was shown as a regulator of both proliferation and apoptosis in keratinocytes (Bernard et al., 2002). Cx26 mutations had similar c-Rel expression in reduced intracellular Ca^{2+} while they had opposite phenotypes, lethality, and proliferation. Compared to WT, they both had lower c-Rel expression in reduced intracellular Ca^{2+}. That showed that G45E and D50Y might show their phenotypes in normal Ca^{2+} homeostasis. Conversely, it has been shown that Ca^{2+} might inhibit c-Rel nuclear localization via CaM (Berry et al., 2018). This is open for further investigation by checking the expression of c-Rel target genes such as cell cycle regulator, p21 (Basile et al., 2003). Similarly, reduction of extracellular Ca^{2+} caused lower expression of c-Rel in WT and D50Y. Even though it was suggested that intracellular Ca^{2+} levels might be restored in reduced extracellular Ca^{2+}, it might not be sufficient for c-Rel expression. The nuclear localization of c-Rel was reduced in G45E and D50Y in reduced extracellular Ca^{2+}. IKK-γ did not reveal significant data to discuss in reduced intracellular Ca^{2+} results but reduction of extracellular did not change IKK-γ expression in WT and D50Y, meaning that IKK-γ expression was independent from Ca^{2+}.

RelB, a member of the non-canonical pathway, did not exhibit a change in WT and D50Y under reduced intracellular conditions but showed lower expression in G45E. Notably, RelB levels were already low in D50Y under physiological conditions. Therefore, the activation of RelB was unaffected by the reduction of intracellular Ca^{2+} in D50Y. RelB activation is known to occur via NIK activation (Bren et al., 2001). Previous studies have demonstrated that intracellular Ca^{2+} is necessary for NIK activation (Mogensen et al., 2003). In the case of G45E, the reduced levels of RelB in response to reduced intracellular Ca^{2+} may be explained by decreased NIK activation. Conversely,

calcineurin (CaN) has been shown to inhibit NIK, p65, and RelB activation (Shinzawa et al., 2015). D50Y also displayed low nuclear localization of RelB, while G45E exhibited high nuclear localization of RelB. To establish the link between intracellular Ca^{2+} and RelB, further investigations into Ca^{2+} or its binding proteins may be warranted. Similarly, as observed in the results of reduced intracellular Ca^{2+}, a significant decrease in RelB was evident in both WT and D50Y when extracellular Ca^{2+} levels were reduced. As mentioned earlier, Ca^{2+} activates NIK and RelB, and the absence of Ca^{2+} may contribute to the marked decrease in WT and D50Y, which already had lower RelB expression under normal physiological conditions. RelB has been identified as upregulated in response to induced intracellular Ca^{2+} and associated with cell survival (Moy et al., 2022).

Here, we investigated varying characteristics of Cx26 KID syndrome mutations through NF-κB pathway activation and expression of NF-κB pathway members. Also, we showed aberrant Ca^{2+} transport through mutated Cx26 hemichannels affected NF-κB activation.

REFERENCES

Aasen, T.; Johnstone, S.; Vidal-Brime, L.; Lynn, K. S.; Koval, M. Connexins: Synthesis, post-translational modifications, and trafficking in health and disease. Int. J. Mol. Sci. 2018, 19(5), 1296.

Abdo, J. M.; Sopko, N. A.; Milner, S. M. The applied anatomy of human skin: A model for regeneration. Wound Med. 2020, 28, 179.

Ahmad, S.; Martin, P. E. M.; Evans, W. H. Assembly of gap junction channels Mechanism, effects of calmodulin antagonists and identification of connexin oligomerization determinants.

Alam, H.; Sehgal, L.; Kundu, S. T.; Dalal, S. N.; Vaidya, M. M. Novel function of keratins 5 and 14 in proliferation and differentiation of stratified epithelial cells. Mol. Biol. Cell 2011, 22(21), 4068–4078.

Al-Ani, A. M.; Messenger, A. G.; Lawry, J.; Bleehen, S. S.; Macneil, S. Calcium/calmodulin regulation of the proliferation of human epidermal keratinocytes, dermal fibroblasts and mouse B16 melanoma cells in culture. Br. J. Dermatol. 1988, 119(6), 697-703.

Antonsson, Å.; Hughes, K.; Edin, S.; Grundström, T. Regulation of c-Rel Nuclear Localization by Binding of Ca2+/Calmodulin. Mol. Cell. Biol. 2003, 23(4), 1418–1427.

Arndt, S.; Aschendorff, A.; Schild, C.; Beck, R.; Maier, W.; Laszig, R.; Birkenhäger, R. A Novel Dominant and a De Novo Mutation in the GJB2 Gene (Connexin-26) Cause Keratitis-Ichthyosis-Deafness Syndrome: Implication for Cochlear Implantation.

Aypek, H.; Bay, V.; Meşe, G. Altered cellular localization and hemichannel activities of KID syndrome associated connexin26 I30N and D50Y mutations. BMC Cell Biol. 2016, 17(1), 10.

Bagur, R.; Hajnóczky, G. Intracellular Ca2+ Sensing: Its Role in Calcium Homeostasis and Signaling. Mol. Cell 2017, 66(6), 780–788.

Bahr, C.; Rohwer, A.; Stempka, L.; Rincke, G.; Marks, F.; Gschwendt, M. DIK, a novel protein kinase that interacts with protein kinase Cδ: Cloning, characterization, and gene analysis. J. Biol. Chem. 2000, 275(46), 36350–36357.

Bargiello, T. A.; Oh, S.; Tang, Q.; Bargiello, N. K.; Dowd, T. L.; Kwon, T. Gating of Connexin Channels by transjunctional-voltage: Conformations and models of open and closed states. Biochim. Biophys. Acta Biomembr. 2018, 1860(1), 22-39. DOI: 10.1016/j.bbamem.2017.04.028

Basile, J. R.; Eichten, A.; Zacny, V.; Mü Nger, K. NF-KB-Mediated Induction of p21 Cip1/Waf1 by Tumor Necrosis Factor A Induces Growth Arrest and Cytoprotection in Normal Human Keratinocytes. AACR Journals. 2003, 1(4), 262-270. Full Text

Bedoukian, E. C.; Rentas, S.; Skraban, C.; Shao, Q.; Treat, J.; Laird, D. W.; Sullivan, K. E. Palmoplantar keratoderma with deafness phenotypic variability in a patient with an inherited GJB2 frameshift variant and novel missense variant. Mol. Genet. Genomic Med. 2021, 9(2). DOI: 10.1002/mgg3.1574

Bernard, D.; Monte, D.; Vandenbunder, B.; Abbadie, C. The c-Rel transcription factor can both induce and inhibit apoptosis in the same cells via the upregulation of MnSOD. Oncogene 2002, 21, 4392-4402. DOI: 10.1038/sj.onc

Berry, C. T.; May, M. J.; Freedman, B. D. STIM- and Orai-mediated calcium entry controls NF-κB activity and function in lymphocytes. Cell Calcium 2018, 74, 131-143. DOI: 10.1016/j.ceca.2018.07.003

Bikle, D. D.; Mauro, T. M. Calcium, orai1, and epidermal proliferation. J. Investig. Dermatol. 2014, 134(6), 1506-1508. DOI: 10.1038/jid.2014.54

Blanpain, C.; Fuchs, E. Epidermal stem cells of the skin. Ann. Rev. Cell Dev. Biol. 2006, 22, 339-373. DOI: 10.1146/annurev.cellbio.22.010305.104357

Bren, G. D.; Solan, N. J.; Miyoshi, H.; Pennington, K. N.; Pobst, L. J.; Paya, C. V. Transcription of the RelB gene is regulated by NF-kB. Nature.com. 2001. Full Text

Campbell, K. J.; O'Shea, J. M.; Perkins, N. D. Differential regulation of NF-κB activation and function by topoisomerase II inhibitors. BMC Cancer 2006, 6. DOI: 10.1186/1471-2407-6-101

Chen, P.; Wu, W.; Zhang, J.; Chen, J.; Li, Y.; Sun, L.; Hou, S.; Yang, J. Pathological mechanisms of connexin26-related hearing loss: Potassium recycling, ATP-calcium signaling, or energy supply? Front. Mol. Neurosci. 2022, 15. DOI: 10.3389/fnmol.2022.976388

Takao, J. T.; Y. T.; D. A.; S. S.; B. M.; A. K.; C. P. D. Cutaneous Biology Expression of NF-jB in epidermis and the relationship between NF-jB activation and inhibition of keratinocyte growth.

Deruy, E.; Gosselin, K.; Vercamer, C.; Martien, S.; Bouali, F.; Slomianny, C.; Bertout, J.; Bernard, D.; Pourtier, A.; Abbadie, C. MnSOD upregulation induces autophagic programmed cell death in senescent keratinocytes. PLoS ONE 2010, 5(9), 1-18. DOI: 10.1371/journal.pone.0012712

Deucher, A.; Efimova, T.; Eckert, R. L. Calcium-dependent involucrin expression is inversely regulated by protein kinase C (PKC)α and PKCδ. J. Biol. Chem. 2002, 277(19), 17032-17040. DOI: 10.1074/jbc.M109076200

Di, Z.; Herpers, B.; Fredriksson, L.; Yan, K.; van de Water, B.; Verbeek, F. J.; Meerman, J. H. N. Automated Analysis of NF-κB Nuclear Translocation Kinetics in High-Throughput Screening. PLoS ONE 2012, 7(12). DOI: 10.1371/journal.pone.0052337

Dobrowolski, R.; Sommershof, A.; Willecke, K. Some oculodentodigital dysplasia-associated Cx43 mutations cause increased hemichannel activity in addition to deficient gap junction channels. J. Membr. Biol. 2007, 219(1-3), 9-17. DOI: 10.1007/s00232-007-9055-7

Donahue, H. J.; Qu, R. W.; Genetos, D. C. Joint diseases: From connexins to gap junctions. Nat. Rev. Rheumatol. 2018, 14(1), 42-51. DOI: 10.1038/nrrheum.2017.204

Donnelly, S.; English, G.; De Zwart-Storm, E. A.; Lang, S.; Van Steensel, M. A. M.; Martin, P. E. Differential susceptibility of Cx26 mutations associated with epidermal dysplasias to peptidoglycan derived from Staphylococcus aureus and Staphylococcus epidermidis. Exp. Dermatol. 2012, 21(8), 592-598. DOI: 10.1111/j.1600-0625.2012.01521.x

Essenfelder, G. M.; Bruzzone, R.; Lamartine, J.; Charollais, A.; Blanchet-Bardon, C.; Barbe, M. T.; Meda, P.; Waksman, G. Connexin30 mutations responsible for hidrotic ectodermal dysplasia cause abnormal hemichannel activity. Hum. Mol. Genet. 2004, 13(16), 1703-1714. DOI: 10.1093/hmg/ddh191

Evans, W. H.; De Vuyst, E.; Leybaert, L. The gap junction cellular internet: Connexin hemichannels enter the signalling limelight. Biochem. J. 2006, 397(1), 1-14. DOI: 10.1042/BJ20060175

Faniku, C.; Wright, C. S.; Martin, P. E. Connexins and pannexins in the integumentary system: The skin and appendages. Cell. Mol. Life Sci. 2015, 72(15), 2937-2947. DOI: 10.1007/s00018-015-1969-0

Fuchs, E. Skin stem cells: Rising to the surface. J. Cell Biol. 2008, 180(2), 273-284. DOI: 10.1083/jcb.200708185

Fullard, N.; Moles, A.; O'Reilly, S.; Van Laar, J. M.; Faini, D.; Diboll, J.; Reynolds, N. J.; Mann, D. A.; Reichelt, J.; Oakley, F. The c-Rel subunit of NF-κB regulates epidermal homeostasis and promotes skin fibrosis in mice. Am. J. Pathol. 2013, 182(6), 2109-2120. DOI: 10.1016/j.ajpath.2013.02.016

Furue, M. Regulation of filaggrin, loricrin, and involucrin by IL-4, IL-13, IL-17A, IL-22, AHR, and NRF2: Pathogenic implications in atopic dermatitis. Int. J. Mol. Sci. 2020, 21(15). DOI: 10.3390/ijms21155382

García, I. E.; Bosen, F.; Mujica, P.; Pupo, A.; Flores-Muñoz, C.; Jara, O.; González, C.; Willecke, K.; Martínez, A. D. From Hyperactive Connexin26 Hemichannels to Impairments in Epidermal Calcium Gradient and Permeability Barrier in the Keratitis-Ichthyosis-Deafness Syndrome. J. Invest. Dermatol. 2016, 136(3), 574-583. DOI: 10.1016/j.jid.2015.11.017

Garcia-Vega, L.; O'shaughnessy, E. M.; Albuloushi, A.; Martin, P. E. Connexins and the Epithelial Tissue Barrier: A Focus on Connexin 26. Biology 2021. DOI: 10.3390/biology

Gerido, D. A.; Derosa, A. M.; Richard, G.; White, T. W. Aberrant hemichannel properties of Cx26 mutations causing skin disease and deafness. Am. J. Physiol. Cell Physiol. 2007, 293, 337-345. DOI: 10.1152/ajpcell.00626.2006

Gerlo, S.; Kooijman, R.; Beck, I. M.; Kolmus, K.; Spooren, A.; Haegeman, G. Cyclic AMP: A selective modulator of NF-κB action. Cell. Mol. Life Sci. 2011, 68(23), 3823-3841. DOI: 10.1007/s00018-011-0757-8

Goodenough, D. A.; Paul, D. L. Gap junctions. Cold Spring Harbor Perspect. Biol. 2009, 1(1). DOI: 10.1101/cshperspect.a002576

Grinberg-Bleyer, Y.; Dainichi, T.; Oh, H.; Heise, N.; Klein, U.; Schmid, R. M.; Hayden, M. S.; Ghosh, S. Cutting Edge: NF-κB p65 and c-Rel Control Epidermal Development and Immune Homeostasis in the Skin. J. Immunol. 2015, 194(6), 2472-2476. DOI: 10.4049/jimmunol.1402608

Gugasyan, R.; Voss, A.; Varigos, G.; Thomas, T.; Grumont, R. J.; Kaur, P.; Grigoriadis, G.; Gerondakis, S. The Transcription Factors c-rel and RelA Control Epidermal Development and Homeostasis in Embryonic and Adult Skin via Distinct Mechanisms. Mol. Cell. Biol. 2004, 24(13), 5733–5745. DOI: 10.1128/mcb.24.13.5733-5745.2004

Havouis, S.; Dumas, G.; Avé, P.; Pritsch, O.; Huerre, M.; Dighiero, G.; Pourcel, C. Mice lacking the transcription factor RelB develop T cell-dependent skin lesions similar to human atopic dermatitis. Eur. J. Immunol. 2000, 30(8), 2323–2332. DOI: 10.1002/1521-4141(2000)30:8<2323::AID-IMMU2323>3.0.CO;2-H

Hershfield, M. S. New insights into adenosine-receptor-mediated immunosuppression and the role of adenosine in causing the immunodeficiency associated with adenosine deaminase deficiency. Eur. J. Immunol. 2005, 35(1), 25–30. DOI: 10.1002/eji.200425738

Hu, Y.; Baud, V.; Oga, T.; Il Kim, K.; Yoshida, K.; Karin, M. IKKa controls formation of the epidermis independently of NF-kB. www.nature.com

Jonard, L.; Feldmann, D.; Parsy, C.; Freitag, S.; Sinico, M.; Koval, C.; Grati, M.; Couderc, R.; Denoyelle, F.; Bodemer, C.; Marlin, S.; Hadj-Rabia, S. A familial case of Keratitis-Ichthyosis-Deafness (KID) syndrome with the GJB2 mutation G45E. Eur. J. Med. Genet. 2008, 51(1), 35–43. DOI: 10.1016/j.ejmg.2007.09.005

Keller, M. D.; Petersen, M.; Ong, P.; Church, J.; Risma, K.; Burham, J.; Jain, A.; Richard Stiehm, E.; Hanson, E. P.; Uzel, G.; Deardorff, M. A.; Orange, J. S. Hypohidrotic ectodermal dysplasia and immunodeficiency with coincident NEMO and EDA mutations. Front. Immunol. 2011, 2(NOV), 1–8. DOI: 10.3389/fimmu.2011.00061

Kim, C.; Pasparakis, M. Epidermal p65/ NF -κB signalling is essential for skin carcinogenesis. EMBO Mol. Med. 2014, 6(7), 970–983. DOI: 10.15252/emmm.201303541

Kotini, M.; Barriga, E. H.; Leslie, J.; Gentzel, M.; Rauschenberger, V.; Schambon, A.; Mayor, R. Gap junction protein Connexin-43 is a direct transcriptional regulator of N-cadherin in vivo. Nat. Commun. 2018, 9(1). DOI: 10.1038/s41467-018-06368-x

Lee, H. J.; Kim, M. Skin Barrier Function and the Microbiome. Int. J. Mol. Sci. 2022, 23(21). DOI: 10.3390/ijms232113071

Lee, S. E.; Lee, S. H. Skin barrier and calcium. Ann. Dermatol. 2018, 30(3), 265–275. DOI: 10.5021/ad.2018.30.3.265

Li, Q.; Lu, Q.; Hwang, J. Y.; Bü, D.; Lee, K.-F.; Carlos Izpisua-Belmonte, J.; Verma, I. M. IKK1-deficient mice exhibit abnormal development of skin and skeleton. www.genesdev.org

Li, Z. J.; Sohn, K. C.; Choi, D. K.; Shi, G.; Hong, D.; Lee, H. E.; Whang, K. U.; Lee, Y. H.; Im, M.; Lee, Y.; Seo, Y. J.; Kim, C. D.; Lee, J. H. Roles of TLR7 in Activation of NF-κB Signaling of Keratinocytes by Imiquimod. PLoS ONE 2013, 8(10). DOI: 10.1371/journal.pone.0077159

Lilly, E.; Sellitto, C.; Milstone, L. M.; White, T. W. Connexin channels in congenital skin disorders. Semin. Cell Dev. Biol. 2016, 50, 4–12. DOI: 10.1016/j.semcdb.2015.11.018

Lilly, E., Strickler, M., Milstone, L. M., & Bunick, C. G. "Alterations in connexin 26 protein structure from lethal keratitis-ichthyosis-deafness syndrome mutations A88V and G45E." J. Dermatol. Sci. 2019, 95(3), 119-122. DOI: 10.1016/j.jdermsci.2019.07.002

Lopez, W., Gonzalez, J., Liu, Y., Harris, A. L., & Contreras, J. E. "Insights on the mechanisms of Ca2+ regulation of connexin26 hemichannels revealed by human pathogenic mutations (D50N/Y)." J. Gen. Physiol. 2013, 142(1), 23-45. DOI: 10.1085/jgp.201210893

Lopez, W., Ramachandran, J., Alsamarah, A., Luo, Y., Harris, A. L., & Contreras, J. E. "Mechanism of gating by calcium in connexin hemichannels." Proc. Natl. Acad. Sci. USA 2016, 113(49), E7986-E7995. DOI: 10.1073/pnas.1609378113

Lorenz, V. N., Schön, M. P., & Seitz, C. S. "C-Rel downregulation affects cell cycle progression of human keratinocytes." J. Invest. Dermatol. 2014, 134(2), 415-422. DOI: 10.1038/jid.2013.315

Mahanty, S., Dakappa, S. S., Shariff, R., Patel, S., Swamy, M. M., Majumdar, A., & Gangi Setty, S. R. "Keratinocyte differentiation promotes ER stress-dependent lysosome biogenesis." Cell Death Dis. 2019, 10(4). DOI: 10.1038/s41419-019-1478-4

Makris. "Female Mice Heterozygous for IKK/NEMO Deficiencies Develop a Dermatopathy Similar to the Human X-Linked Disorder Incontinentia Pigmenti."

Mese, G., Sellitto, C., Li, L., Wang, H. Z., Valiunas, V., Richard, G., Brink, P. R., & White, T. W. "The Cx26-G45E mutation displays increased hemichannel activity in a mouse model of the lethal form of keratitis-ichthyosis-deafness syndrome." Mol. Biol. Cell 2011, 22(24), 4776-4786. DOI: 10.1091/mbc.E11-09-0778

Mitchell, J. P., & Carmody, R. J. "NF-κB and the Transcriptional Control of Inflammation." Int. Rev. Cell Mol. Biol. 2018, 335, 41-84. DOI: 10.1016/bs.ircmb.2017.07.007

Mogensen, T. H., Melchjorsen, J., & Paludan, S. R. "Activation of NF-B in Virus-Infected Macrophages Is Dependent on Mitochondrial Oxidative Stress and Intracellular Calcium: Downstream Involvement of the Kinases TGF-Activated Kinase 1, Mitogen-Activated Kinase/Extracellular Signal-Regulated Kinase Kinase 1, and IB Kinase 1." J. Immunol. 2003, 170.

Moy, R. H., Nguyen, A., Loo, J. M., Yamaguchi, N., Kajba, C. M., Santhanam, B., Ostendorf, B. N., Wu, Y. G., Tavazoie, S., & Tavazoie, S. F. "Functional genetic screen identifies ITPR3/calcium/RELB axis as a driver of colorectal cancer metastatic liver.

Ng, D. C., Shafaee, S., Lee, D., & Bikle, D. D. "Requirement of an AP-1 Site in the calcium response region of the involucrin promoter." J. Biol. Chem. 2000, 275(31). DOI: 10.1074/jbc.M002508200

Oeckinghaus, A., & Ghosh, S. "The NF-kappaB family of transcription factors and its regulation." Cold Spring Harbor Perspect. Biol. 2009, 1(4). DOI: 10.1101/cshperspect.a000034

Page, A., Navarro, M., Garín, M., Pérez, P., Casanova, M. L., Moreno, R., Jorcano, J. L., Cascallana, J. L., Bravo, A., & Ramírez, A. "IKKB leads to an inflammatory skin disease resembling interface dermatitis." J. Invest. Dermatol. 2010, 130(6), 1598-1610. DOI: 10.1038/jid.2010.28

Pani, B., & Singh, B. B. "Darier's disease: A calcium-signaling perspective." Cell. Mol. Life Sci. 2008, 65(2), 205-211. DOI: 10.1007/s00018-007-7397-z

Pease, L. I., Wordsworth, J., & Shanley, D. "Transcriptomic and epigenetic assessment of ageing female skin and fibroblasts identifies age-related reduced oxidative phosphorylation exacerbated by smoking." DOI: 10.1101/2022.08.16.504111

Peled, A., Sarig, O., Sun, G., Samuelov, L., Ma, C. A., Zhang, Y., Dimaggio, T., Nelson, C. G., Stone, K. D., Freeman, A. F., Malki, L., Vidal, L. S., Chamarthy, L. M., Briskin, V., Mohamad, J., Pavlovsky, M., Walter, J. E., Milner, J. D., & Sprecher, E. "Loss-of-function mutations in caspase recruitment domain-containing protein 14 (CARD14) are associated with a severe variant of atopic dermatitis." J. Allergy Clin. Immunol. 2019, 143(1), 173-181.e10. DOI: 10.1016/j.jaci.2018.09.002

Pflug, K. M., & Sitcheran, R. "Targeting NF-κB-inducing kinase (NIK) in immunity, inflammation, and cancer." Int. J. Mol. Sci. 2020, 21(22), 1-19. DOI: 10.3390/ijms21228470

Rebholz, B., Haase, I., Eckelt, B., Paxian, S., Flaig, M. J., Ghoreschi, K., Nedospasov, S. A., Mailhammer, R., Debey-Pascher, S., Schultze, J. L., Weindl, G., Förster, I., Huss, R., Stratis, A., Ruzicka, T., Röcken, M., Pfeffer, K., Schmid, R. M., & Rupec, R. A. "Crosstalk between Keratinocytes and Adaptive Immune Cells in an IκBα Protein-Mediated Inflammatory Disease of the Skin." Immunity 2007, 27(2), 296-307. DOI: 10.1016/j.immuni.2007.05.024

Richard, G., Rouan, F., Willoughby, C. E., Brown, N., Chung, P., Ryynänen, M., Jabs, E. W., Bale, S. J., Digiovanna, J. J., Uitto, J., & Russell, L. "Missense Mutations in GJB2 Encoding Connexin-26 Cause the Ectodermal Dysplasia Keratitis-Ichthyosis-Deafness Syndrome." Am. J. Hum. Genet 2002, 70.

Sánchez, H. A., Meşe, G., Srinivas, M., White, T. W., & Verselis, V. K. "Differentially altered Ca2+ regulation and Ca2+ permeability in Cx26 hemichannels formed by the A40V and G45E mutations that cause keratitis ichthyosis deafness syndrome." J. Gen. Physiol. 2010, 136(1), 47-62. DOI: 10.1085/jgp.201010433

Scott, C. A., Tattersall, D., O'Toole, E. A., & Kelsell, D. P. "Connexins in epidermal homeostasis and skin disease." Biochim. Biophys. Acta - Biomembranes 2012, 1818(8), 1952-1961. DOI: 10.1016/j.bbamem.2011.09.004

Seitz, C. S., Deng, H., Hinata, K., Lin, Q., & Khavari, P. A. "Nuclear Factor B Subunits Induce Epithelial Cell Growth Arrest 1." Cancer Res. 2000, 60. Link

Sellitto, C., Li, L., & White, T. W. "Connexin hemichannel inhibition ameliorates epidermal pathology in a mouse model of keratitis ichthyosis deafness syndrome." Sci. Rep. 2021, 11(1). DOI: 10.1038/s41598-021-03627-8

Shen, Y., Boulton, A. P. R., Yellon, R. L., & Cook, M. C. "Skin manifestations of inborn errors of NF-κB." Front. Pediatr. 2023, 10. DOI: 10.3389/fped.2022.1098426

Shinzawa, M., Konno, H., Qin, J., Akiyama, N., Miyauchi, M., Ohashi, H., Miyamoto-Sato, E., Yanagawa, H., Akiyama, T., & Inoue, J. I. "Catalytic subunits of the phosphatase calcineurin interact with NF-κB-inducing kinase (NIK) and attenuate NIK-dependent gene expression." Sci. Rep. 2015, 5. DOI: 10.1038/srep10758

Srinivas, M., Verselis, V. K., & White, T. W. "Human diseases associated with connexin mutations." Biochim. Biophys. Acta - Biomembranes 2018, 1860(1), 192-201. DOI: 10.1016/j.bbamem.2017.04.024

Sun, L., & Carpenter, G. "Epidermal growth factor activation of NF-kB is mediated through IkBa degradation and intracellular free calcium." Link

Tran, G., Nhieu, V., Clair, C., Bruzzone, R., Mesnil, M., Sansonetti, P., & Combettes, L. "Connexin-dependent inter-cellular communication increases invasion and dissemination of Shigella in epithelial cells." Nat. Cell Biol. 2003, 5(8).

Tu, C. L., Crumrine, D. A., Man, M. Q., Chang, W., Elalieh, H., You, M., Elias, P. M., & Bikle, D. D. "Ablation of the calcium-sensing receptor in keratinocytes impairs epidermal differentiation and barrier function." J. Invest. Dermatol. 2012, 132(10), 2350-2359. DOI: 10.1038/jid.2012.159

Vičanová, J., Boelsma, E., Mommaas, A. M., Kempenaar, J. A., Forslind, B., Pallon, J., Egelrud, T., Koerten, H. K., & Ponec, M. "Normalization of Epidermal Calcium Distribution Profile in Reconstructed Human Epidermis Is Related to Improvement of Terminal Differentiation and Stratum Corneum Barrier Formation."

Weber, P. A., Chang, H. C., Spaeth, K. E., Nitsche, J. M., & Nicholson, B. J. "The permeability of gap junction channels to probes of different size is dependent on connexin composition and permeant-pore affinities." Biophys. J. 2004, 87(2), 958-973. DOI: 10.1529/biophysj.103.036350

Weih, F., Durham, S. K., Barton, D. S., Sha, W. C., Baltimore, D., & Bravo, R. "p50-NF-B Complexes Partially Compensate for the Absence of RelB: Severely Increased Pathology in p50 / relB / Double-knockout Mice." J. Exp. Med. 1997, 185(7). Link

Wittwer, T., & Schmitz, M. L. "NIK and Cot cooperate to trigger NF-κB p65 phosphorylation." Biochem. Biophys. Res. Commun. 2008, 371(2), 294-297. DOI: 10.1016/j.bbrc.2008.04.069

Wong, P., Tan, T., Chan, C., Laxton, V., Chan, Y. W. F., Liu, T., Wong, W. T., & Tse, G. "The role of connexins in wound healing and repair: Novel therapeutic approaches." Front. Physiol. 2016, 7(DEC). DOI: 10.3389/fphys.2016.00596

Wullaert, A., Bonnet, M. C., & Pasparakis, M. "NF-κB in the regulation of epithelial homeostasis and inflammation." Cell Res. 2011, 21(1), 146-158. DOI: 10.1038/cr.2010.175

Yamamoto, N., Tanigaki, K., Han, H., Hiai, H., & Honjo, T. "Notch/RBP-J Signaling Regulates Epidermis/Hair Fate Determination of Hair Follicular Stem Cells." Curr. Biol. 2003, 13.

Yong, L., Yu, Y., Li, B., Ge, H., Zhen, Q., Mao, Y., Yu, Y., Cao, L., Zhang, R., Li, Z., Wang, Y., Fan, W., Zhang, C., Wang, D., Luo, S., Bai, Y., Chen, S., Chen, W., Liu, M., … Sun, L. "Calcium/calmodulin-dependent protein kinase IV promotes imiquimod-induced psoriatic inflammation via macrophages and keratinocytes in mice." Nat. Commun. 2022, 13(1). DOI: 10.1038/s41467-022-31935-8

Zhang, Q., Lenardo, M. J., & Baltimore, D. "30 Years of NF-κB: A Blossoming of Relevance to Human Pathobiology." Cell 2017, 168(1–2), 37-57. DOI: 10.1016/j.cell.2016.12.012